Aircraft ice-nucleating particle and aerosol composition measurements in the western North American Arctic

Alberto Sanchez-Marroquin[1], Sarah L. Barr [1], Ian T. Burke[1], James B. McQuaid[1], Benjamin J. Murray[1] (*)

[1]School of Earth and Environment, University of Leeds, Woodhouse Lane, Leeds, LS2 9JT, UK

(*) Corresponding author: b.j.murray@leeds.ac.uk

Knowledge of the temperature dependent concentration of ice-nucleating particles (INPs) is crucial to understanding the properties of mixed-phase clouds. However, the sources, transport and removal of INPs around the globe, and particularly in the Arctic region, are poorly understood. In the Arctic winter and spring, when many local sources are covered by ice and snow, it is not clear which INP types are important. In this study, we present a new dataset of aircraft-based immersion mode INP measurements and aerosol size-resolved composition in the western North American Arctic from the 11th – 21st March 2018. Aerosol samples were collected between ~70 and 600 m above the surface on filters that were analysed using both a freezing droplet-based assay and Scanning Electron Microscopy with Energy Dispersive Spectroscopy (SEM-EDS). The measured INP concentrations were at or close to the limit of detection, with concentrations at -20°C of 1 L^{-1} or below. The size-resolved composition measurements indicates that the aerosol concentrations were low, dominated mostly by sea spray aerosol and mineral dust. Further analysis shows that mineral dust is important for the ice-nucleating properties of our samples, dominating over the sea spray aerosol particles in the four cases we analysed, suggesting that mineral dust is a relevant source of INPs in the Alaskan springtime Arctic. Furthermore, the INP concentrations are more consistent with fertile soil dusts that have an ice active biological component than what would be expected for the ice-active mineral K-feldspar alone. While we cannot rule out local high latitude sources of dust, the relatively small size of the mineral dust implies that the dust was from distant sources.

1. Introduction

Clouds containing both supercooled liquid water and ice are known as mixed-phase clouds and they reflect a substantial amount of the incoming solar shortwave radiation that reaches the Earth (Boucher, 2013). The lifetime, as well as the amount of radiation that these clouds reflect, is strongly affected by the partitioning between liquid and ice (Storelvmo et al., 2015). When above temperatures required for homogeneous freezing (below ~-35°C), ice formation in mixed-phase clouds is initiated by the presence of a small fraction of the aerosol particles known as ice-nucleating particles (INPs) (Murray et al., 2012). Once ice crystals nucleate, they can grow more rapidly than liquid cloud droplets since ice has a lower equilibrium vapour pressure than supercooled water. This process can lead to the precipitation of the ice crystals, removing liquid water from a cloud (Korolev et al., 2017;Vergara-Temprado et al., 2018;Hawker et al., 2021). Ice-related processes in mixed-phase clouds such as the primary production of ice and the link to INP concentration are commonly oversimplified in climate models, which contributes to large discrepancies in the amount of water and ice that the models simulate (Komurcu et al., 2014;McCoy et al., 2016;McCoy et al., 2018). The difficulty of properly representing the current

45 water and ice mixing state of these clouds is responsible for the large uncertainty of the cloud-phase
46 feedback (Storelvmo et al., 2015).

47 As the atmosphere warms, mixed-phase clouds will contain more supercooled water leading to a
48 reduction in shortwave radiation reaching the surface, but also decrease the outgoing longwave radiation
49 flux (Ceppi et al., 2017;Murray et al., 2021). Hence, mixed-phase mid- to high-latitude clouds over the
50 ocean have a negative feedback (Tan et al., 2016), whereas clouds over high albedo ice or snow covered
51 surfaces have a positive feedback (Tan et al., 2016). The strength of these feedbacks depends on the
52 balance between ice and supercooled water in these clouds both in the present and future climate. Hence,
53 better understanding the sources and concentrations of atmospheric INPs, particularly at the mid- to
54 high-latitudes could help to reduce the uncertainty associated with cloud feedbacks.

55 Only a small fraction of aerosol particles have the potential to become INPs. Transported dust from the
56 deserts is one of the most important sources of worldwide atmospheric INPs, especially at temperatures
57 below -15 °C (Hoose and Mohler, 2012;Vergara-Temprado et al., 2017;Kanji et al., 2017). Given the
58 fact that substantial amounts of dust are transported from the deserts to the Arctic (Fan, 2013;Huang et
59 al., 2015;Francis et al., 2018), this dust could contribute to the INP population of the region (Irish et al.,
60 2019;Yun et al., 2022). Additionally, local sources of high-latitude dust are known to contribute to the
61 dust budget in the Arctic (Bullard et al., 2016;Groot Zwaaftink et al., 2016;Meinander et al., 2022;Shi
62 et al., 2021). Some of these sources of high-latitude dust have been found to contribute to the Arctic
63 INP population (Tobo et al., 2019;Sanchez-Marroquin et al., 2020;Si et al., 2019). A fraction the INP
64 in the Arctic are also of biogenic origin (Wex et al., 2019;Porter et al., 2022), some of which may be
65 associated with biogenic material in sea spray and some of which may be from terrestrial sources
66 (Wilson et al., 2015;DeMott et al., 2016;Vergara-Temprado et al., 2017;Irish et al., 2017;McCluskey et
67 al., 2018;Bigg and Leck, 2001;Creamean et al., 2019;Hartmann et al., 2020;Creamean et al., 2020).
68 Biogenic material attached to dust particles could be an important part of these terrestrial INPs
69 (O'Sullivan et al., 2014;O'Sullivan et al., 2015;Tobo et al., 2019). Other types of aerosol particles such
70 as volcanic ash or biomass burning particles could also contribute to the INP population in the Arctic
71 (Prenni et al., 2009).

72 The available literature data indicates that the INP concentrations in the Arctic are highly variable,
73 depending on the season and location (Murray et al., 2021). Using samples from land-based sites around
74 the Arctic collected over several years, Wex et al. (2019) found that Arctic INP concentrations reach a
75 minimum during winter, but they increase through spring and reach a maximum around the summer,
76 suggesting that concentrations are highest when the transport of aerosol from the low latitudes is at its
77 weakest (the summer). Similarly, year-round measurements in the central Arctic indicate peak
78 concentrations in the summer months of 2020 (Creamean et al., 2022). Creamean et al. (2022) suggested
79 that local Arctic marine sources might contribute to the elevated INP populations in the summer. Porter
80 et al. (2022) also found elevated summertime INP concentration, during August 2018, while in the pack
81 ice near the North Pole. However, in contrast to Creamean et al. (2022), Porter et al. (2022) concluded
82 that these very active INPs were associated with air masses originating from lower latitude ice-free
83 regions along the Russian coast, whereas air masses that had spent the preceding week or so over ice-
84 covered surfaces (in the central Arctic pack ice) had very low INP particle concentrations . The central
85 Arctic in 2018 and 2020 appear to be rather different, with Porter et al. (2022) reporting up to 2 L^{-1} at -
86 15°C in 2018, whereas Creamean et al. (2022) reported two orders of magnitude lower peak INP
87 concentrations in 2020. Hence, there may simply be a great deal of variability and the contrasting
88 conclusions between Porter et al. (2022) and Creamean et al. (2022) may be appropriate for their
89 respective study periods. Creamean et al. (2018) found a similar trend in INP concentrations to Wex et
90 al. (2019) over spring, with coarse particles being responsible for the higher INP concentration event.
91 However, a recent study did not find strong seasonality of Arctic INPs at Ny-Ålesund, although these
92 measurements were limited to being between April and August 2018 (Rinaldi et al., 2021). Furthermore,
93 there have been very few INP measurements from aircraft. Given there are strong aerosol sinks in the

94   boundary layer, whereas the air above the boundary layer can be stratified with corresponding long
95   aerosol lifetimes (Carslaw, 2022), vertical measurements are required. Hartmann et al. (2020) report
96   INP spectra for late March and early April north of 80° over the Fram Strait and Arctic Ocean and report
97   that the highest INP concentrations (2×10^{-2} L^{-1} at -15°C) correspond to the boundary layer, indicating
98   a local marine source even though the region was mostly ice covered. Overall, the picture of INP
99   concentrations in the Arctic is that of high variability, both spatially and temporal (on days to years
100 timescales), with the potential for high variability in local sources, transport from lower latitudes as
101 well as in local INP sinks.

102 In this paper, we present a set of immersion mode INP and aerosol size-resolved composition
103 measurements carried out in the western North American Arctic during March 2018 using an aircraft.
104 Our measurements were carried out at different altitudes up to ~ 600 m above sea level both within and
105 above the boundary layer. INP measurements were combined with aerosol characteristics determined
106 using SEM-EDS to indicate the types of INPs that are were most important during this campaign.

107

2. Sampling location and methods

Aerosol particles were sampled from the UK's BAe-146 FAAM atmospheric research aircraft during the Measurements of Arctic Cloud, Snow and Sea Ice in the Marginal Ice ZonE (MACSSIMIZE) campaign, based in Fairbanks, Alaska (US) in March 2018. The majority of the measurements were carried out close to the northern coast of Alaska and the Canadian territory of Yukon, both over land and over the Arctic Ocean, as shown in Fig. 1, where the flight track corresponding to each sample has been presented. Measurements were carried out at altitudes between 40 and 600 m above sea level, as detailed in Table 1 along with other pertinent information. Some filters were collected in a single run on a constant heading and height, while others were collected over several runs, with the filters system mostly closed during turns between the runs and altitude changes, although this was not possible for all filters. Filters were collected over 9 to 36 minutes, which at a science speed of ~360 km hr^{-1} corresponded to a horizontal distance of between ~50 and ~200 km. All the sampling was done outside of cloud and precipitation.

Aerosol particles were collected using the filter inlet system on board of the FAAM BAe-146, which has been characterised by Sanchez-Marroquin et al. (2019). Briefly, this inlet is located outside the skin of the FAAM BAe-146 and brings aerosol particles to a filter located inside the cabin with a 45° angle bend. The sampling occurs in sub-isokinetic conditions, which enhances coarse mode aerosol particles. Sampling efficiency for particles with diameters above 20 μm becomes very small due to inertial losses in the system (at the bend). No treatment (heat or drying) is applied to the sampled airmass, although the cabin was warmer than the ambient air in this campaign and hence the RH of air passing through the inlet system once inside the aircraft is therefore very low. The system allowed us to collect two aerosol samples in parallel: one on a polycarbonate filter (Whatman Nuclepore polycarbonate track-etched filters, 47 mm diameter with a pore size of 0.4 μm) and one on a Teflon filter (Sartorius polytetrafluoroethylene, 47 mm diameter with a pore size of 0.45 μm). For these filter types, the particle collection efficiency is likely to be close to 100 % for the relevant size ranges, as discussed in Sanchez-Marroquin et al. (2019) using the data of Soo et al. (2016) and Lindsley (2016).

The ice-nucleating particle assay was conducted in a temporary laboratory set up in a hotel room near the aircraft base in Fairbanks, Alaska, with minimum time between sampling and analysis. Most filters were analysed a matter of hours after collection, however where this was not possible they were stored at ~ -18 $^{\circ}$C for a few days prior to analysis. This approach has a number of advantages compared to the commonly used strategy of bringing filters back to a laboratory for latter analysis. Firstly, analysis of field blanks can reveal sources of contamination that can be reduced by making adjustments to the experimental protocol; secondly, we can try to adjust the sampling methodology (such as sampling time) to fit the INP concentration and thirdly, we can minimise storage and transport of filters thus reducing potential biases. Teflon filters were used to perform a droplet-on-filter freezing assay to quantify the INP concentration, as described in detail in Price et al. (2018) and also used by Sanchez-Marroquin et al. (2020) and (Sanchez-Marroquin et al., 2021). The technique was first described by Schnell (1982) and our version of this assay makes use of the Asymptote EF600 Stirling cooler described in Whale et al. (2015). For the present study we pipetted 2 μL pure water droplets on top of each filter that had been exposed to aerosol particles (or handling blanks). On average, we pipetted 54 (with and standard deviation of 5) droplets per filter. The filters were placed on top of a cold stage, within a chamber that is flushed with dry nitrogen gas to prevent water condensation, that is cooled at a constant rate of 1 $^{\circ}$C min^{-1} until temperatures of ~-35 $^{\circ}$C. Droplet freezing was recorded and the resulting videos were manually analysed to determine the fraction of droplets frozen at each temperature and then the INP concentration. At least one handling blank experiment was performed for every flight. Handling blank filters were prepared and transported in the same way as the measurement filters including loading the filters into the sampling system on the aircraft and briefly opening (for a second or so) and closing the inlet valves that allow air to pass through the filters. Hence, the handling blank should provide information on sources of contamination throughout the handling of the filter. A

disadvantage of the droplet-on-filter technique is that each sample can only be analysed once, which makes it incompatible with standard heat tests such as the ones described by Daily et al. (2022). However, the great advantage of the droplet-on-filter technique over techniques where particles are washed off a filter into a volume of water is that it is around 20 times more sensitive than a typical wash-off assay employing 1 μL droplets (depending on the details of the freezing assays). This enhanced sensitivity is very important given that aerosol sampling durations are typically only a few tens of minutes long.

The droplet fraction frozen (the fraction of droplet that were frozen as a function of temperature) produced by our samples, along with those produced by the handling blank filters, is shown in Fig 2a. While the fraction frozen for the sample filters were generally shifted to warmer temperatures than the handling blanks, many of the samples overlapped with the range defined by the handling blanks. Hence it was necessary to account for influence of the background from the measurements. The background subtraction procedure and the INP concentration calculations are detailed in Appendix A. Briefly, we converted our cumulative fraction frozen values for the samples and handling blanks into the differential INP spectrum, $k(T)$, in units of INP per unit temperature (Vali, 1971;Vali, 2019). k is the number of INP that become active in a temperature interval. This allowed us to define a limit of detection then apply a criterion to separate samples that show a significant signal above this from the ones that do not. Data points whose error bars did not overlap with the error bars associated to the handling blank were considered to be above the limit of detection. The error bars of the differential concentrations of the samples represent a confidence level of 68 % while the error bars of the background represents the standard deviation of all the measured handling blanks. Background-subtraction was applied to data points above the limit of detection($k_{sample} - k_{background}$) using a similar approach to Vali (2019). The cumulative INP spectrum, the common way of presenting INP data, was then derived using the background corrected values of k.

A subset of the polycarbonate filters was analysed using Scanning Electron Microscopy with Energy Dispersive Spectroscopy (SEM-EDS) to study aerosol size-resolved composition. The analysis was carried out in the Leeds Electron Microscopy And Spectroscopy centre (LEMAS), at the University of Leeds. Filters were transported to the University of Leeds and then stored at ~-18 $^{\circ}$C until its analysis. This technique can be used to obtain the morphological and chemical properties of individual aerosol particles within the sample. The subset of samples was coated with a 30 nm layer of Iridium and the SEM-EDS analysis was performed using an accelerating voltage of 20 KeV. The scanning and acquisition of EDS spectrums is done using a semi-automatic method with the Aztec Feature Software by Oxford Instruments. Our method captures the morphology and chemical signature of particles down to 0.2 or 0.3 μm, depending on the sample. Particles are detected based on their contrast in the secondary electron images, although some artefacts were removed manually. Each particle is then classified into a defined composition category based on its chemical composition. The morphological and composition category of each particles is used to obtain statistics about the size-resolved composition of the aerosol samples. A more detailed description of the technique can be found in Sanchez-Marroquin et al. (2019).

In parallel with the filters sampling, we make use of FAAM's underwing optical particle counters. One of these counters is the Passive Cavity Aerosol Spectrometer Probe 100-X (PCASP), manufactured by Particle Measurement Systems, and measures aerosol particles in the 0.1 to ~3 μm range. The second counter is the Cloud Droplet Probe (CDP) by Droplet Measurement Technologies and it measures aerosol particles and droplets with sizes from ~3 to 50 μm. A detailed description of these instruments and its calibration and can be found in Rosenberg et al. (2012).

The Hybrid Single-Particle Lagrangian Integrated Trajectory (HYSPLIT) model was used to calculate five day back trajectories of sampled air masses (Stein et al., 2015;Rolph et al., 2017) and shown in Sect S1. The back trajectories show that in many cases air masses remained near or over Alaska and northern Canada before sampling. However, the backtrajectories corresponding to the C085 flight

205 arrived mostly from the south west. Most of the trajectories suggest that the air mostly stayed at altitudes
206 below 1000 m above sea level in the five days prior to sampling. At the time of sampling, most of the
207 sea and land surfaces were covered by sea ice or snow (Fig. 1), which most likely suppressed any local
208 aerosol sources. However, local sources of marine aerosol particles may still occur due to open leads
209 (May et al., 2016;Kirpes et al., 2019;Chen et al., 2022).

3. INP concentrations in the western North American Arctic

212 The background corrected cumulative INP concentrations are shown in Fig 2b. Hollow markers indicate
213 measurements consistent with the limit of detection, where the lower error bar goes to zero, while filled
214 markers correspond to a cumulative INP concentration above the limit of detection. Using a 68 %
215 confidence interval, approximately 70 % of the differential spectra binned data was not significantly
216 above the limit of detection and around half of the data points in the cumulative INP spectra shown in
217 Fig. 2b show INP concentrations consistent with zero (i.e. not above the detection limit). The reported
218 INP concentrations are always below 0.1 and 1 L^{-1} at -15 $^{\circ}$C and -20 $^{\circ}$C, respectively. However, given
219 the fact that a substantial percentage of the data is not above the detection limit, the real values of some
220 of these samples may be well below these values. A daily, more detailed representation of the INP
221 concentrations is shown in Fig. B3.

222 INP concentrations across the Arctic vary significantly depending on the time of the year and location
223 (Creamean et al., 2018;Si et al., 2019;Wex et al., 2019). Hence, in order to compare to the pertinent
224 data we show our INP concentrations alongside literature data collected in a similar location and time
225 of the year in Fig. 3a (we restricted the literature datasets from February to April). Some of our reported
226 INP concentrations are above some of the values measured using a droplet freezing assay on filters
227 collected the surface by Creamean et al. (2018) and Wex et al. (2019) as well as filters collected on an
228 aircraft and processed using a dynamic developing chamber at water saturation by Borys (1989).
229 Creamean et al. (2018) reported INP concentrations at -25 $^{\circ}$C up to 0.1 L^{-1} on the north coast of Alaska
230 in March. Measurements performed by Wex et al. (2019) in a close location (Utqiaġvik) indicate that
231 INP concentrations ranging from ~10^{-4} to 10^{-2} L^{-1} at -10 $^{\circ}$C in March. The more active samples reported
232 by Wex et al. (2019) form a consistent INP spectrum with our more active samples, but unfortunately
233 there is no direct overlap. Borys (1989) reported INP concentrations of 0.001 L^{-1} to 0.3 L^{-1} at -25 $^{\circ}$C
234 measured from an aircraft at a similar location and time of the year. These values are of course consistent
235 with our samples where we report upper limits, but some of our samples clearly had substantially higher
236 INP concentrations than the range reported by Borys (1989). Hiranuma et al. (2013) also report INP
237 measurements using an airborne continuous flow diffusion chamber (CFDC) during the Indirect and
238 Semi-Direct Aerosol Campaign (ISDAC) in a very similar study region to ours, but in April rather than
239 March. We have only compared our measurements with theirs at water saturation, which happened to
240 be during a relatively high INP period. This INP value of 5.6 ± 3.5 L^{-1} at -22°C is consistent with our
241 highest recorded INP concentrations. Overall, this comparison with measurements in previous years at
242 a similar location and time of year indicates that the INP concentrations are rather variable, ranging
243 over at least three orders of magnitude at -20°C.

244 Our measurements have also been presented alongside a compilation of INP measurements from across
245 the Arctic carried out throughout the year (Fig 3b). Our dataset is well within the range of literature INP
246 measurements from across the Arctic. Around 50% of our data points were below detection limit (and
247 not shown in Fig. 3), hence we are only able to report INP concentrations when their values are
248 relatively high. The picture that emerges in the Arctic is a region of highly variable INP concentrations,
249 where INP concenrations vary spatialy as well as temporally (seasonaly as well as on shorter time
250 scales). This variability is likely related to a combination of transport from local and remote sources of
251 INP as well as sinks both locally and along those transport routes. This high variability in INP
252 concentrations will affect primary ice production in clouds, with more INP leading to greater ice

253 concentrations that may or may not be amplified by secondary production processes. Intriguingly,
254 several authors report that greater INP concentrations leads to more ice in Arctic cloud and vice versa
255 (Rogers et al., 2001;Hiranuma et al., 2013).

256 A handful of measurements of INP have been made from aircraft (Hartmann et al., 2020;Sanchez-
257 Marroquin et al., 2020;Prenni et al., 2009;Hiranuma et al., 2013) and it is these measurements that
258 produce many of the highest observed Arctic INP concentrations, rather than those made on the ground.
259 However, aircraft sampling is often limited by the volume of air that can be sampled due to restrictions
260 in flight lengths and other technical limitations. This necessarily biases the results to relatively high INP
261 concentrations. For example, (Rogers et al., 2001) report that 50% of the 10 s averaged data was zero
262 (i.e. below detection limit). Given the Arctic atmosphere is highly stratified, it would be interesting to
263 perform simultaneous measurements at the surface and from an aircraft to explore how or if INP at the
264 surface are related to those higher in the boundary later and those in the free troposphere.

265

4. SEM-EDS size-resolved composition analysis

267 The equivalent circular diameter size distributions obtained with the SEM-EDS technique were
268 compared with the average size distributions for the same sampling periods measured using the
269 underwing optical particle counters on-board of the FAAM BAe-146. The analysis is shown in Fig. 4
270 alongside the size-resolved chemical composition of the analysed samples. The number size distribution
271 is multiplied by the fraction of particles in each category and binned to calculate the number size
272 distribution of each category. Then these number size distributions are turned into surface area size
273 distributions and integrated to obtain the surface area of each category, as shown in Table 2.

274 The analysed samples exhibited low aerosol concentrations relative to other locations where we have
275 used this technique, especially for the coarse mode. In this study, almost no particles above 10 μm were
276 detected, in contrast to samples from around Iceland, the eastern tropical Atlantic and the south east of
277 the United Kingdom analysed using the same or similar technique, where significant amounts of
278 aerosols in between 10 and 20 μm were detected (Price et al., 2018;Sanchez-Marroquin et al.,
279 2019;Sanchez-Marroquin et al., 2020;Sanchez-Marroquin et al., 2021). Most of the detected particles
280 were below ~2 μm. At sizes below ~3 μm, the comparison between the optical probes and the SEM-
281 EDS size distributions are consistent in most cases, with an undercounting at the lower end of the SEM-
282 EDS technique (~0.3 μm). This undercounting is related to the difficulty in observing small organic rich
283 particles and has been discussed in Sanchez-Marroquin et al. (2019). At sizes above ~3 μm, the optical
284 probes and SEM-EDS size distributions showed a comparable amount of detected particles in samples
285 C089_3 and C090_1. However, for samples C087_1 and C091_2, the optical counters detected a larger
286 concentration of particles with sizes ~5 to 10 μm than the SEM analysis of the filters. Similar
287 discrepancies have been observed previously with these instruments in another low aerosol environment
288 (Young et al., 2016), and were attributed to regions of high humidity even if the average humidity in a
289 run should not have led to substantial hygroscopic growth. In dust plumes near Iceland and in aerosol
290 around the UK where there was a significant coarse mode the agreement between CDP and SEM tended
291 to be good. We note CDP is designed for cloud droplets, and we are using it at the edge of its capability
292 for larger aerosol particles, hence there may be some biases which seem more significant in low aerosol
293 environments.

294 In terms of chemical composition, the samples were mainly dominated by sea spray (Na rich) and
295 mineral dust (Si rich, Si only, Al-Si rich and Ca rich) particles. There were some smaller contributions
296 of S rich particles (likely sulphates) and Carbonaceous particles (likely black carbon or organic
297 material). This is consistent with other SEM-EDS studies of the aerosol samples collected on the
298 Alaskan Arctic from the ground (Chen et al., 2022;Creamean et al., 2018;Kirpes et al., 2018;Gunsch et
299 al., 2017) or during a ship campaign (Kirpes et al., 2020). However, we tend to observe larger fractions

300 of dust aerosol particles, particularly in the sample C090_1, where this type of aerosol constituted ~65
301 % of the surface area of the sample.

302 In this dataset, nearly all particles in the Na rich category were dominated by the presence of Na and
303 Cl, having traces of other elements (such as S in some occasions), consistent with sea spray particles.
304 As a consequence, we will refer to particles in this category as sea spray aerosol particles. Some
305 carbonaceous particles were also detected through most sizes and there were significant contributions
306 of S rich aerosol, particularly in the accumulation mode. As shown in Fig. 4 and Table 2, the surface
307 area of samples C087_1 and C091_2 were dominated by sea spray aerosol particles with sizes around
308 ~ 1 μm. In Sect. S1 it is shown that most of the air masses associated with these samples had been
309 circulating above the Arctic Ocean at relatively low altitude (below 1000 m) before sampling took place.
310 This is consistent with the fact that sea spray aerosol particles are normally emitted by bubble bursting
311 in the surface of the oceans (Lewis and Schwartz, 2004). It is possible that the detected sea spray aerosol
312 in our study was transported from ice free oceans. However, Sect. S1 indicates that the closest ocean
313 masses were almost fully covered by sea ice (with some open leads) during the campaign and the
314 majority of the sampled air masses did not pass by the open oceans prior to sampling. Hence, it is
315 possible that the sea spray particles had been emitted from open leads in the sea ice, as this is thought
316 to be a source of sea spray aerosol in the region (May et al., 2016;Kirpes et al., 2019;Chen et al., 2022).
317 It is also possible that some of the sea spray aerosol has been directly emitted from the sea ice through
318 blowing snow events (Yang et al., 2008;Huang and Jaeglé, 2017;Frey et al., 2020).

319 Particles in the categories Si rich, Si only, Al-Si rich and Ca rich have a chemical composition consistent
320 with mineral dust particles so we will refer to them collectively as mineral dust. However, it should be
321 borne in mind that the composition of particles in these categories is also consistent with some types of
322 combustion ashes or volcanic ash. Mineral dust particles were present in all the samples, particularly
323 with sizes between 1 and 5 μm, constituting a substantial percentage of its surface area, as shown in
324 Table 2. This was particularly the case in the sample C090_1, where 65 % of the surface area was given
325 by mineral dust particles. Although we cannot fully determine the relative contribution of different
326 sources to the detected mineral dust, several arguments suggest that the sampled mineral dust originated
327 from the low latitude deserts. The back trajectory analysis shown in Sect. S1 suggests that most of the
328 air masses had been circulating around the sampling location prior to sampling for ~5 days. However,
329 the majority of the potential high-latitude dust sources were covered by snow at this time, so it seems
330 unlikley that this mineral dust is related to natural emissions, although we cannot rule out sources
331 associated with human activities along the coast (e.g. Purdue Bay oil fields). Mineral dust originating
332 from the Sahara and Central Asia is known to be transported to the Arctic, especially in late winter and
333 early spring, when this study took place (VanCuren et al., 2012;Fan, 2013;Huang et al., 2015;Francis
334 et al., 2018;Shi et al., 2022;Zhao et al., 2022). This is consistent with the some of the backtrajectories
335 associated to the samples collected on the C085 flight, which originate from Asia. Almost all the mineral
336 dust particles found in this study had sizes below 5 μm and it is known that dust particles have a lifetime
337 of many days so can conceivably be transported to Alaska from distant sources (Huneeus et al.,
338 2011;Ménégoz et al., 2012). Once in the Arctic, accumulation mode aerosol has a lifetime extending to
339 months during winter and spring, when removal processes are weak (Carslaw, 2022). The small sizes
340 of dust particles found in this campaign contrast with results obtained using similar techniques on
341 samples collected closer to dust sources, where dust particles with sizes above 10 μm are frequent (Price
342 et al., 2018;Ryder et al., 2018;Sanchez-Marroquin et al., 2020). Although this evidence suggests that
343 most of our dust likely originated in arid lower-latitude deserts, high-latitude dust could still contribute
344 to the dust budget or even dominate it during other times of the year such as autumn (Groot Zwaaftink
345 et al., 2016;Shi et al., 2022).

346 As shown in Table 2, C087_1 and C091_2 samples have a larger surface area of sea spray aerosol
347 particles (Na rich) than mineral dust, whereas sample C090_1 is dominated by the presence of mineral
348 dust. Hence, it is reasonable to ask if the mineral dust or organic material associated with sea spray is

the more important INP type in these samples. To estimate the relative contribution of mineral dust and sea spray aerosol to the INP population, we present the expected INP concentrations based on the SEM-EDS surface areas in Fig. 5, in comparison with the measured INP concentrations. The INP concentrations expected from the SEM-EDS analysis were calculated assuming a dust containing 10 % of K-feldspar (Harrison et al., 2019) (the ice active component of desert dust) and the parametrization of fertile soils given by O'Sullivan et al. (2014). Note that the latter is very similar to the desert dust parameterization given by Ullrich et al. (2017). For the pristine sea spray INP, the parametrization given by McCluskey et al. (2018) that links INP concentration and aerosol surface area has been used. As shown, even in the cases where there is more sea spray aerosol than mineral dust (C087_1 and C091_2), the minimum contribution of mineral dust INP is orders of magnitude above the INPs produced by the pristine sea spray aerosol particles. It is possible that the sea spray in this location was more active than defined by McCluskey et al. (2018), however, the INP concentrations calculated based on the presence of dusts better explains the observed INP concentrations measured using the droplet freezing assay at the lower end of the temperature spectrum. At the higher end of the temperature spectrum, the measured INP concentrations are above those expected from a 10 % K-feldspar dust, but are consistent with the fertile soil dust parameterisation. It is known that fertile soil dusts contain biological ice nucleating material (O'Sullivan et al., 2014), hence this suggests that the samples from Alaska contained some biological ice nucleating material (either from marine or terrestrial sources). Although our INP concentrations would also be comparable with those predicted using the desert dust parameterization by Ullrich et al. (2017), the latter is usually higher than the activity of samples of airborne desert dust at temperatures greater than about -20°C from other studies (Boose et al., 2016;Price et al., 2018;Harrison et al., 2022;Reicher et al., 2018;Gong et al., 2020). It has been suggested that dust that has been transported far from its source regions is less active than arid soil dusts that have been recently aerosolised and also there appears to be substantial differences in activity of dust from different source regions (Boose et al., 2016;Harrison et al., 2022). Hence, we suggest that the enhanced ice-nucleation ability of our samples is perhaps due to the presence of biological material. This is consistent with other studies that also provided evidence that Arctic INP samples have a substantial biological component (Wex et al., 2019;Creamean et al., 2019;Santl-Temkiv et al., 2019;Porter et al., 2022).

5. Conclusions

In this study, we present a new dataset of INP and SEM-EDS aerosol size-resolved composition measurements in the western North American Arctic in March 2018. Back trajectory analysis suggests that most of these air masses spend the preceding five days circulating over or near Alaska and Northern Canada where local sources of primary aerosol were supressed by snow and ice cover. Observed INP concentrations were at or close to the limit of detection of the measuring technique, being always below 0.1 and 1 L^{-1} at – 15 ^{o}C and -20 ^{o}C respectively. SEM-EDS analysis revealed that samples are mostly dominated by the presence of mineral dust and sea spray aerosol particles, with some contributions of sulphur rich and carbonaceous particles. The mineral dust is most likely sourced from the low-latitudes, rather than local high-latitude dust sources. Our analysis shows that mineral dust contributes more to the INP population than sea spray, despite sea spray being more abundant in some samples. However, it appears that the ice-active mineral K-Feldspar cannot account for all of the observed INPs, especially above ~ -22°C. This suggests that there is another INP type that controls the INP spectrum above -22°C; these particles may be biogenic in origin, but where this biogenic ice nucleating material might be derived from is unclear. More work is clearly required to understand the sources and nature of INP in the winter and early springtime Arctic.

Acknowledgments

We are grateful to all the people involved in the MACSSIMIZE campaign, led by Chawn Harlow (UK Met Office). The samples were collected using the FAAM BAe-146-301 Atmospheric Research Aircraft, flown by Airtask Ltd., maintained by Avalon Aero Ltd., and managed by FAAM Airborne Laboratory, jointly operated by UKRI and the University of Leeds. We acknowledge the Centre for Environmental Data Analysis for the access to the FAAM datasets used here. We would also like to thank Duncan Hedges and Richard Walshlaw at the Leeds Electron Microscopy and Spectroscopy Centre.

Author contributions

Aerosol measurements during the MACSSIMIZE campaign were organised by ASM, JBM, and BJM. ASM and BJM worked on the manuscript with contributions from all authors. The field work was carried out by ASM and JBM. ASM performed all the experimental measurements (INP analysis and SEM-EDS). The SEM-EDS technique was developed by ASM and ITB. The back-trajectory analysis was carried out by SLB and ASM. All the authors contributed to the discussion.

Financial support

This research has been supported by the European Research Council (MarineIce (grant no. 648661)) and the Natural Environment Research Council (NE/R006687/1, NE/T00648X/1).

Competing interests

The authors declare that they have no competing interests.

Data and materials availability

All data needed to evaluate the conclusions in the paper are present in the paper and/or the Supplementary Materials. The digitalized data are available from Alberto Sanchez-Marroquin and Benjamin J. Murray (2023): Data for 'Aircraft ice-nucleating particle and aerosol composition measurements in the western North American Arctic '. [Dataset]. https://doi.org/10.5518/1401. FAAM data associated to each of the flights can be found in: Facility for Airborne Atmospheric Measurements; Natural Environment Research Council; Met Office (2018): FAAM C085 MACSSIMIZE flight: Airborne atmospheric measurements from core and non-core instrument suites on board the BAE-146 aircraft. Centre for Environmental Data Analysis. https://catalogue.ceda.ac.uk/uuid/b04281cc10c44d9dab1eb2e4eb19d5b8 (and similar for the other samples).

Sample	Date (2018)	Start time (UTC)	End time (UTC)	GPS altitude (m)	Radar altitude (m)	BL or FT	Vol. PC (L)	Vol. tef. (L)	PTFE position	Stored	Temperature (°C)	Dew temperature (°C)	Aerosol concentration (cm-3)
C085_1	03/11th	22:22	22:34	475	474	FT	466	312	Up	No	-11.1	-14.4	-
C085_3	03/11th	23:18	23:40	604	546	FT	461	355	Low	No	-5.4	-10.6	-
C086_1	03/13th	21:14	21:22	38	38	BL	212	159	Low	No	-16.8	-	76.4
C086_2	03/13th	21:29	21:49	138	139	BL	231	143	Up	No	-17.9	-18.3	75.9
C086_3	03/13th	22:11	22:31	386	387	Intersection	644	209	Low	No	-11.3	-14.1	35.3
C087_1	03/16th	20:44	21:26	310	309	BL	1047	565	Low	No	-19.7	-	68.9
C087_2	03/16th	21:33	22:03	304	305	BL	965	447	Up	No	-16.4	-	61.2
C087_3	03/16th	22:30	22:44	536	491	FT	392	217	Low	Yes	-13.6	-	46.8
C089_1	03/18th	18:01	18:42	584	522	FT *	1198	714	Low	No	-21.3	-20.2	40.3
C089_2	03/18th	18:49	19:17	573	506	FT *	-	398	Low	No	-21.2	-19.3	45.2
C089_3	03/18th	19:28	19:48	591	557	FT *	404	214	Up	Yes	-20.9	-18.8	47.7
C090_1	03/20th	20:15	20:38	547	487	FT *	735	349	Low	No	-15	-15.4	62.1
C090_2	03/20th	20:53	21:26	563	503	FT *	488	409	Up	No	-14.6	-15.6	62.3
C091_2	03/21th	18:27	18:56	122	123	FT *	1187	376	Up	No	-28	-	63.6
C091_3	03/21th	19:01	19:14	295	297	FT *	644	203	Low	Yes	-25.7	-	63.9
C091_4	03/21th	19:21	19:51	71	68	FT *	635	635	Up	No	-29.8	-27.4	31.8

430 Table 1. Details of the samples collected during the MACSSIMIZE campaign. PTFE position
431 refers to which inlet was used to collect the PTFE sample in each run. The other line was used
432 to collect the polycarbonate sample. In order to determine if the sample was collected within
433 the boundary layer (BL) or in the Free Troposphere (FT), we looked at the temperature and
434 potential temperature profiles. (*) For all the runs in the C089, C090 and C091, the flight did
435 not descend low enough to determine the exact depth of the BL. Hence, it was assumed that
436 the runs occurred above the BL. Stored filters were kept for a few hours or days at -18 °C,
437 while the rest of them were analysed immediately after collection without any long-term
438 storage. The given altitude values correspond to the average of each run. The mean values of
439 the air temperature across the run was derived from the Rosemount de-iced temperature
440 sensor, while the dew temperature is given by the Buck CR2 Hygrometer of the BAe-146.
441 Dew temperature could not be calculated for all runs due to technical problems. The aerosol
442 number concentration corresponds to the range of ~0.1 to ~3 μm and it has been calculated
443 using the PCASP instrument. Blank entries correspond to a filter that was not collected or the
444 instruments not working.

445

446
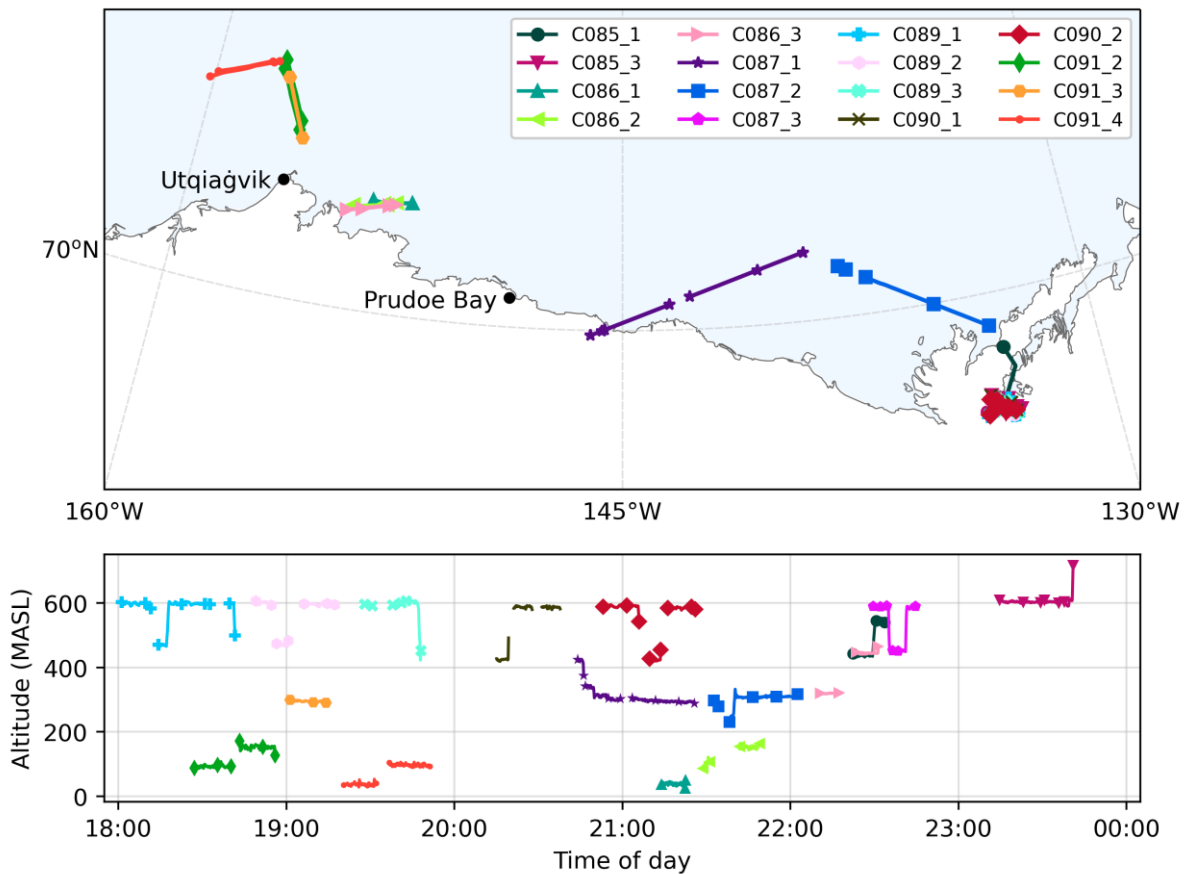
Figure 1. Flight tracks of the samples collected in this study and described in Table 1 (top panel). GPS altitude at which the samples were collected (lower panel). The altitude is presented against the GTM time at which the samples were collected (although they were collected across several days).

450

451
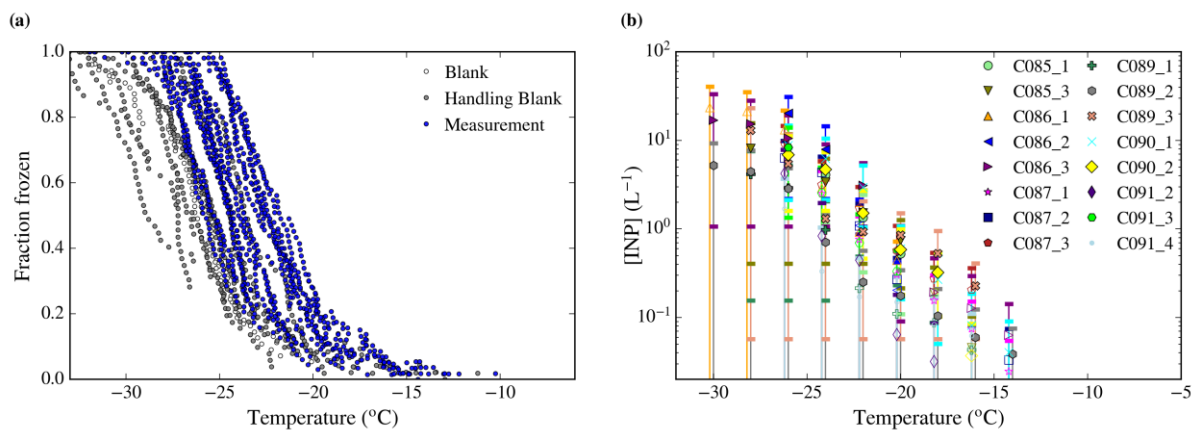
Figure 2. (a) Fraction of droplets frozen for all filter samples as well as blanks and handling blanks. (b) INP particle concentrations for each filter sample. Data points corresponding to the upper limits (open symbols) have been shifted 0.2 ℃ along the x-axis for clarity. The way in which the INP concentrations, upper limits and its uncertainties have been calculated are shown in Appendix A. The criteria to determine if a measurement is above the limit of detection is based on 68% confidence intervals.

457
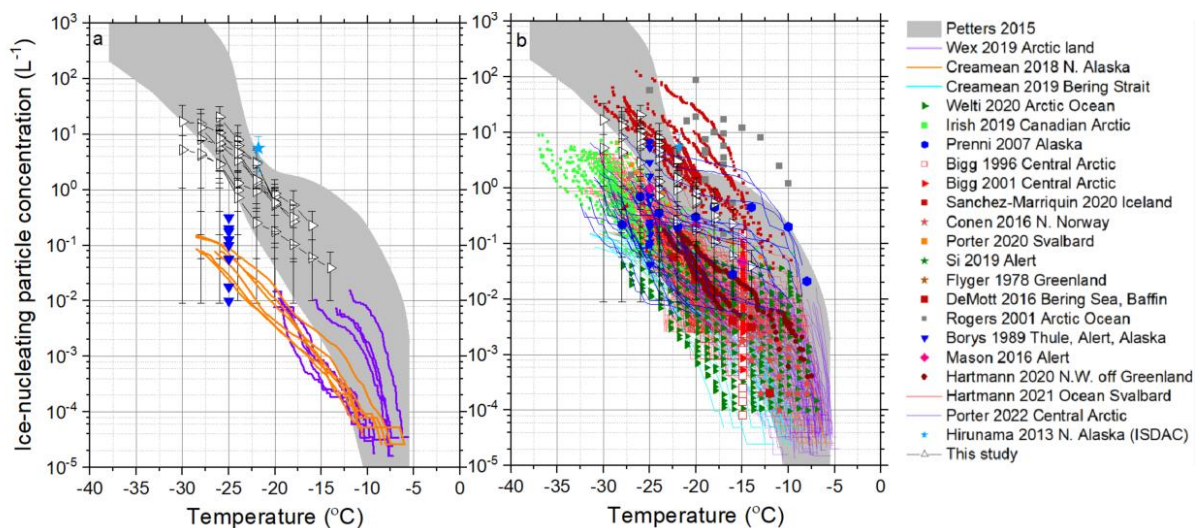
Figure 3. INP concentrations from the present study compared with literature data. We only show our data that was above the background (limiting values are included in Figure 2). Note that this data is above the limit of detection based on 68% confidence intervals. The left panel is limited to a comparison with previous measurements at nearby locations at a similar time of year (February, March and April) (Borys, 1989;Creamean et al., 2018;Wex et al., 2019;Hiranuma et al., 2013). We also limit this comparison to data recorded at or above water saturation, which limits the data from Hiranuma et al. (2013) to a single point during what they describe as a relatively high INP concentration event. Note that for the dataset of Wex et al. (2019), the concentrations increased through this period with the two highest INP spectra from April. The right hand figure is a comparison with Arctic data in general, from any time of the year and any location (Flyger and Heidam, 1978;Borys, 1989;Bigg, 1996;Rogers et al., 2001;Bigg and Leck, 2001;Prenni et al., 2007;Hiranuma et al., 2013;Conen et al., 2016;DeMott et al., 2016;Mason et al., 2016;Creamean et al., 2018;Wex et al., 2019;Creamean et al., 2019;Irish et al., 2019;Si et al., 2019;Porter et al., 2020;Sanchez-Marroquin et al., 2020;Welti et al., 2020;Hartmann et al., 2020;Hartmann et al., 2021;Porter et al., 2022). The mid-latitude data range given by Petters and Wright (2015) is also shown.

478

479

480

481
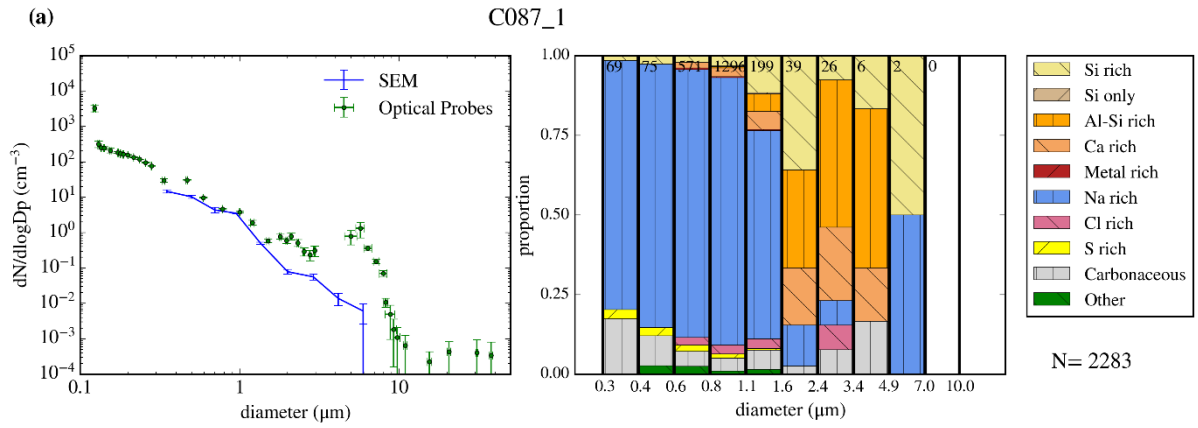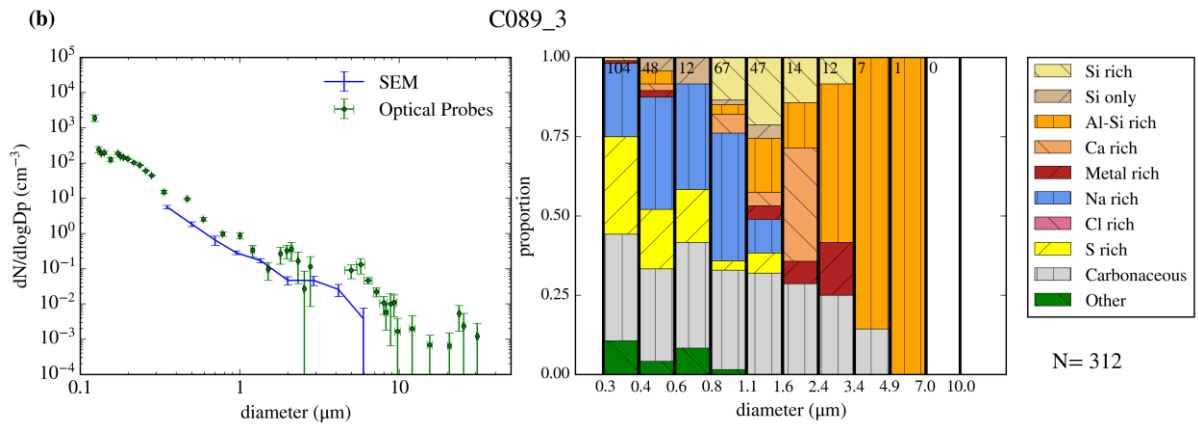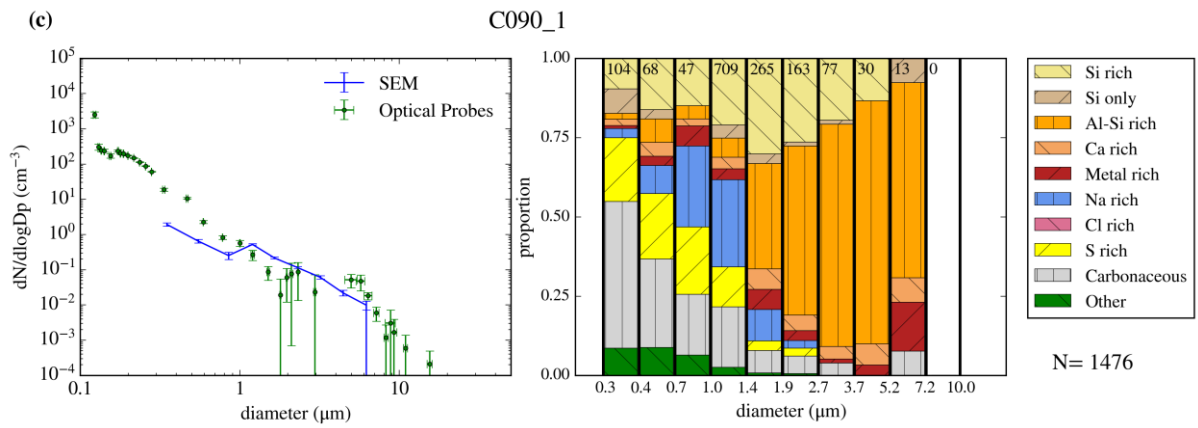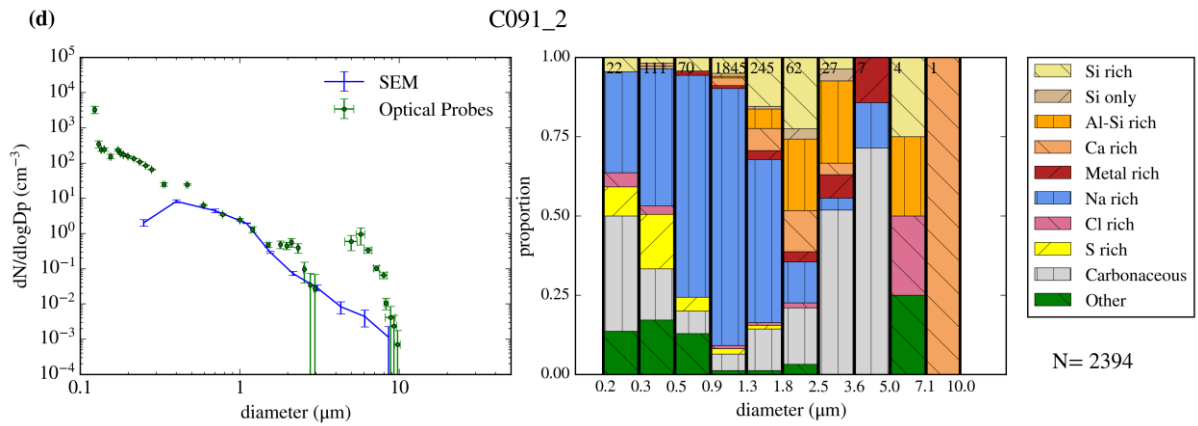
Figure 4. Results of SEM-EDS analysis of each analysed sample (a-d) showing comparison between SEM-EDS and PCASP-CDP number size distribution (left) alongside number size-resolved composition fractions (right).

Sample	Dust area (µm²/cm³)	Dust limit of detection (µm²/cm³)	Dust area percentage	Sea spray aerosol area (µm²/cm³)	Sea spray area percentage
C087_1	0.75	0.042	13.9	3.97	73.4
C089_3	0.57	0.15	38.1	0.26	17.1
C090_1	1.21	0.083	65.5	0.16	8.9
C091_2	0.53	0.051	11.3	2.79	59.5

Table 2. Surface area of dust and sea spray aerosol from SEM-EDS analysis. The dust limit of detection corresponds to the upper limit of the dust concentration detected on the handling blank filter based on one standard deviation. Note that the given dust and sea spray aerosol percentages refer to surface area percentages. The limit of detection of sea spray aerosol particles has not been indicated because the presence of this type of particles in the handling blank is negligible. Further information on the size-resolved composition of the handling blanks and a discussion about it can be found in (Sanchez-Marroquin et al., 2019).
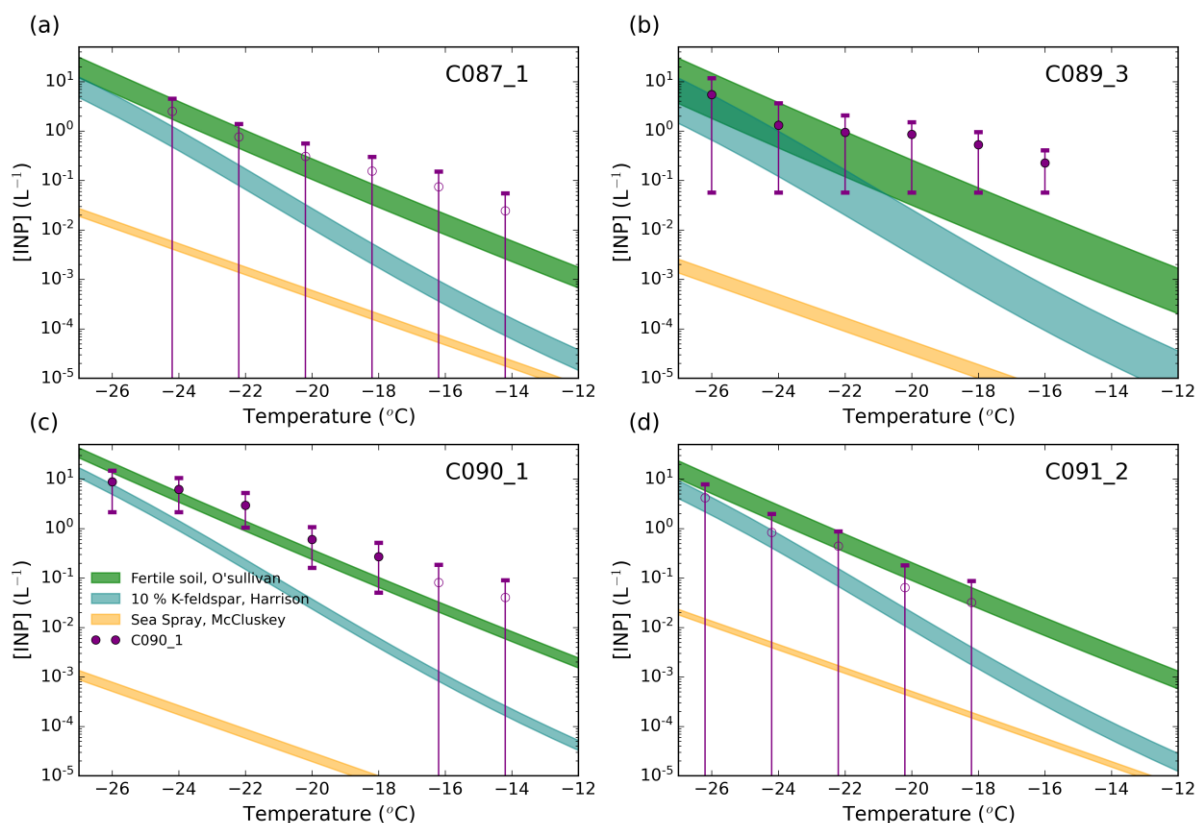
Figure 5. Predicted INP concentration of the SEM-EDS samples compared with the INP measurements at -20 °C. The dust INP prediction has been calculated by applying different ice-nucleation parametrizations to the surface area of dust calculated from the SEM-EDS analysis. The O'Sullivan et al. (2014) for fertile soils and a dust containing 10 % of K-Feldspar (Harrison et al., 2019) have been used. The NaCl INP prediction has been obtained by applying the sea spray aerosol parametrization

501 from McCluskey et al. (2018) to the SEM-EDS sea spray aerosol surface area. The purple points
502 correspond to our INP measurements or upper limits, based on 68% confidence intervals (Appendix A).

503

Appendix A: Upper limit determination and background subtraction of the ice-nucleation experiments

506 As shown in Fig. 2a, most of the fraction of droplets frozen produced by the collected samples were
507 comparable or only slightly above to the ones produced by the handling blanks. Hence, we established
508 criteria to separate data points of the INP spectrum that are not significantly above the limit of detection
509 of the instrument. The analysis is performed using the differential spectrum of ice-nucleus rather than
510 the cumulative spectrum, which is normally used to display and compare ice-nucleation data such as
511 INP concentrations and densities of active sites (Vali, 1971;Vali, 2019). First, we create a histogram
512 with the number of freezing events per temperature interval per sample. This is done for all the samples
513 and handling blanks, with temperature intervals of 2 ^{o}C. We transform the number of freezing events
514 per interval of each sample into the differential INP spectrum, $k(T)$, using Eq. 1 (Vali, 2019).

$$k(T) = -\frac{1}{V\Delta T} ln\left(1 - \frac{\Delta N}{N(T)}\right)$$

Eq. 1

515 In Eq. 1, V is the droplet volume, ΔT is the temperature interval, ΔN is the number of frozen droplets
516 between T and $(T\text{-}\Delta T)$, and $N(T)$ is the number of unfrozen droplets at T. The $k(T)$ values of the handling
517 blanks is shown in Fig B1, alongside the mean value of each interval and its standard deviation. Note
518 that many of the temperature intervals had zero freezing events, corresponding to k equal to zero. These
519 zero values cannot be seen in Fig. B1 but they have been included in the means and standard deviations.
520 The mean and standard deviation of the k values produced by each handling blank has been compared
521 with the k values corresponding to each sample. The uncertainty in the k values associated with each
522 sample has been calculated using a very similar Monte Carlo simulation as used previously (Vali, 2019)
523 using a 68 % interval. The k values associated to each sample were individually compared with the
524 mean and standard deviation of the k values of the handling blanks. A data point was considered above
525 the limit of detection when its lower error yields above the mean plus standard deviation of the blanks.
526 Background subtraction was applied to data points significantly above the limit of detection. This was
527 done by subtracting the mean of the k values of the handling blanks. The error of the background-
528 subtracted point was calculated by square rooting the quadratic sum of the error of the k_{sample} and
529 $k_{background}$. Two examples of the comparisons between samples and the handling blanks are shown in
530 Fig. B2. (a) corresponds to a case where no data point was higher than the limit of detection, while (b)
531 corresponds to a case where most of the data points were significantly above the limit of detection. Note
532 that all the data measured on the 16th of March (flight C087) has been flagged as an upper limit. This is
533 because the handling blank experiment carried out on that day was unusually high, being compatible
534 with all the measurements.

535 The background corrected $k(T)$ was integrated into the cumulative spectrum of active sites, $K(T)$, using
536 Eq. 2 (Vali, 1971;Vali, 2019).

$$K(T) = \sum_{T=0}^{T} k\left(T\right)\Delta T$$

Eq. 2

537 INP concentrations were calculated from , $K(T)$ using Eq. 3, where V_d is the droplet volume, A_{filt} is the
538 area of the filter, V_a is the sampled air volume and α is the contact surface of the droplets. For this study,
539 we used the same values than Sanchez-Marroquin et al. (2021).

$$INP(T) = \frac{K(T)V_D A_{fil}}{V_a \alpha}$$

Eq. 3

540   A *k* value which was not significantly above the limit of detection has been represented with lower bars
541   going to zero in the INP spectrum (meaning upper limit to the INP concentration). However, if a *k* value
542   not significantly above the limit of detection was preceded by a value which was above the limit of
543   detection, then as a result of the cumulative nature of the reported INP concentration the corresponding
544   value is reported with a filled symbol, but the lower bound of the error bar does not change since it is
545   possible that no new INP were present in that temperature interval. In Fig B3 one can see the INP
546   concentration of all the samples collected in this study per each day.

547
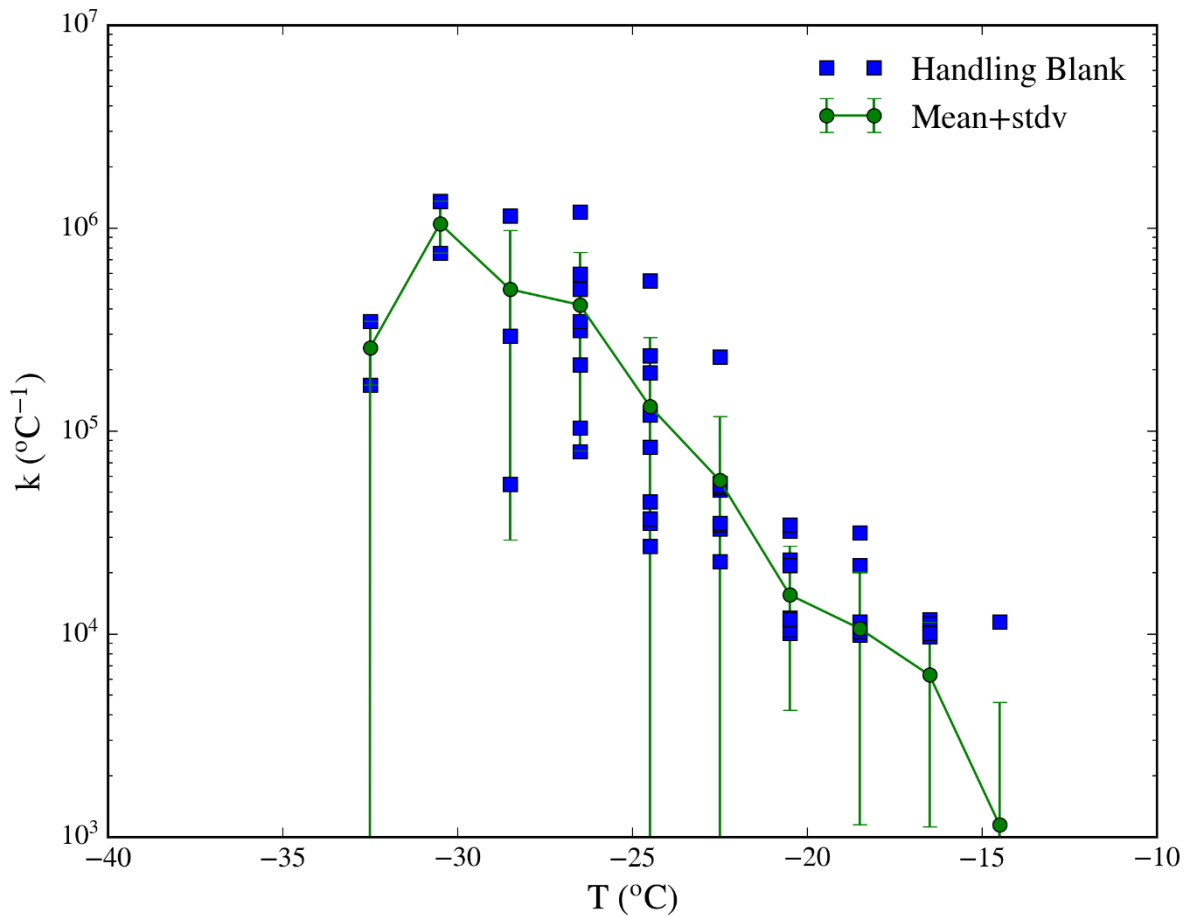
548

549   Figure B1. Differential spectrum of ice-nucleus of all the handling blanks performed during this
550   campaign. Data is shown in blue, while the mean and standard deviation of the data of each bin are
551   show in green.

552

553

554
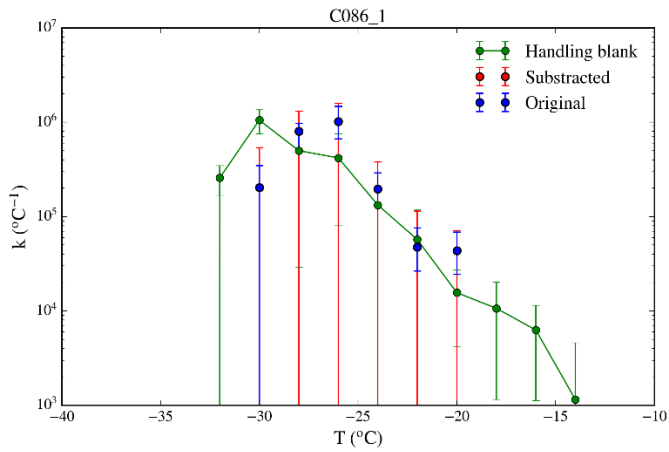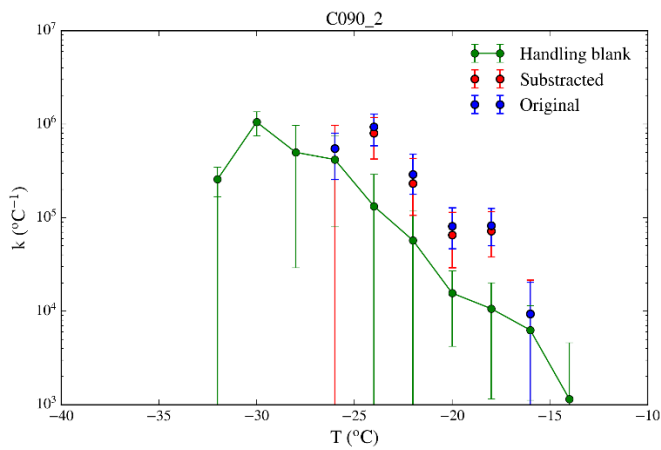
Figure B2. Examples of a comparison between the handling blank mean with two samples. None of the data points of sample C086_1 is significantly above the background. However, most of the data points associated with sample C090_2 are more than one error bar above the data produced by the handling blanks and they have been background-subtracted.
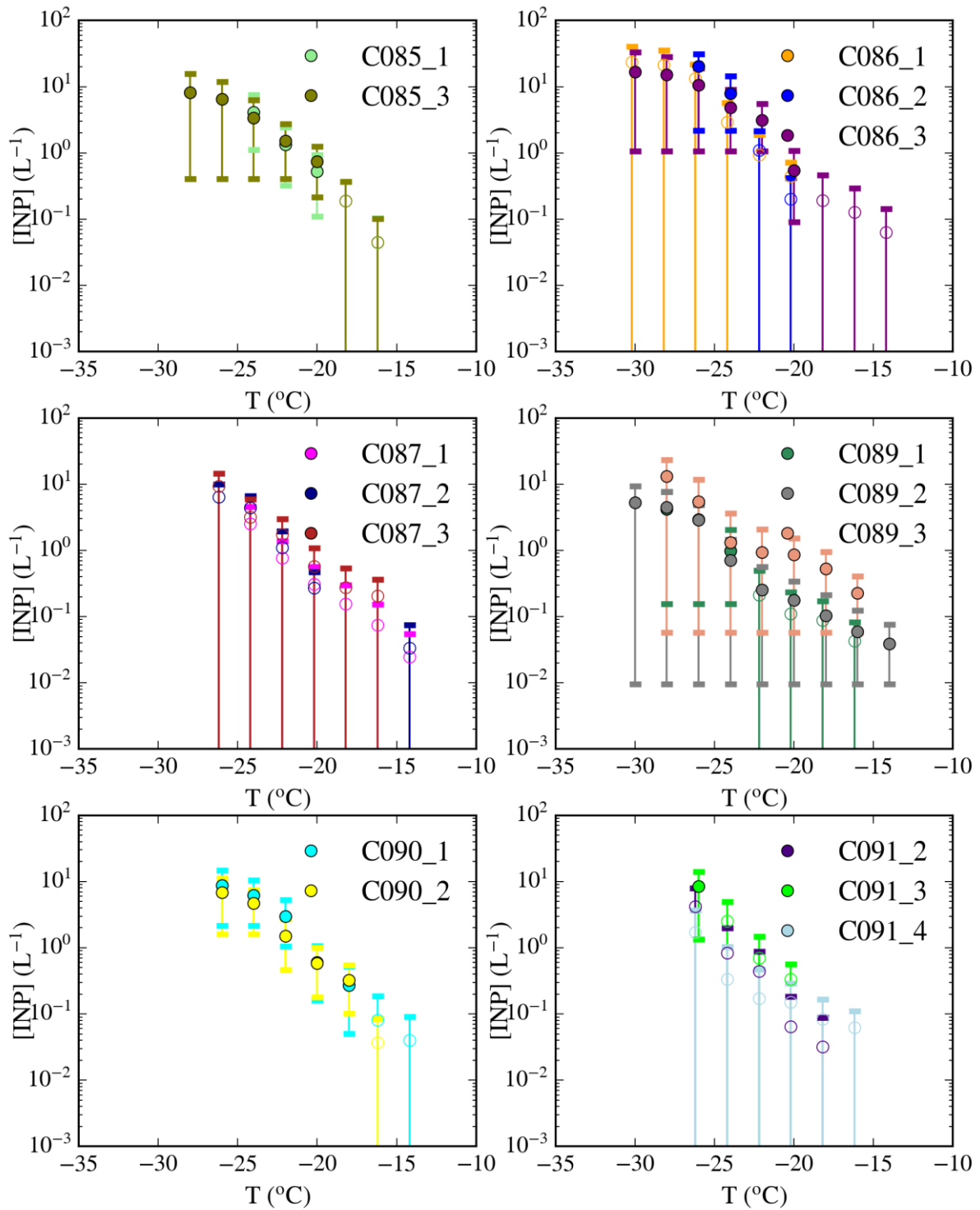
559
560 Fig B3. INP concentrations and upper limits shown in Fig. 2 separated per sampling day. A list of the
561 days when these samples were collected is shown in Table 1. Note that full markers corresponds to
562 measurements above the limit of detection, while hollow markers correspond to upper limits. This has
563 not been specified in the legend as some samples have both upper limits and measurements at the same
564 time.

References

574 **References**

575 Bigg, E. K.: Ice forming nuclei in the high Arctic, Tellus B, 48, 223-233, 10.1034/j.1600-0889.1996.t01-
576 1-00007.x, 1996.

577 Bigg, E. K., and Leck, C.: Cloud-active particles over the central Arctic Ocean, J. Geophys. Res. Atmos.,
578 106, 32155-32166, 10.1029/1999jd901152, 2001.

579 Boose, Y., Sierau, B., García, M. I., Rodríguez, S., Alastuey, A., Linke, C., Schnaiter, M., Kupiszewski, P.,
580 Kanji, Z. A., and Lohmann, U.: Ice nucleating particles in the Saharan Air Layer, Atmos. Chem. Phys,
581 16, 9067-9087, 10.5194/acp-16-9067-2016, 2016.

582 Borys, R. D.: Studies of ice nucleation by Arctic aerosol on AGASP-II, J. Atmos. Chem., 9, 169-185,
583 10.1007/bf00052831, 1989.

584 Boucher, O., D. Randall, P. Artaxo, C. Bretherton, G. Feingold, P. Forster, V.-M. Kerminen, Y. Kondo,
585 H. Liao, U. Lohmann, P. Rasch, S.K. Satheesh, S. Sherwood, B. Stevens and X.Y. Zhang, 2013: Climate
586 Change 2013: The Physical Science Basis. Contribution of Working Group I to the Fifth Assessment
587 Report of the Intergovernmental Panel on Climate Change, in, edited by: [Stocker, T. F., D. Qin, G.-K.
588 Plattner, M. Tignor, S.K. Allen, J. Boschung, A. Nauels, Y. Xia, V. Bex and P.M. Midgley (eds.)],
589 Cambridge University Press, Cambridge, United Kingdom and New York, NY, USA, 2013.

590 Bullard, J. E., Baddock, M., Bradwell, T., Crusius, J., Darlington, E., Gaiero, D., Gassó, S., Gisladottir,
591 G., Hodgkins, R., McCulloch, R., McKenna-Neuman, C., Mockford, T., Stewart, H., and Thorsteinsson,
592 T.: High-latitude dust in the Earth system, Rev Geophys, 54, 447-485, 10.1002/2016rg000518, 2016.

593 Carslaw, K. S.: Chapter 5 - Aerosol processes, in: Aerosols and Climate, edited by: Carslaw, K. S.,
594 Elsevier, 135-185, 2022.

595 Ceppi, P., Brient, F., Zelinka, M. D., and Hartmann, D. L.: Cloud feedback mechanisms and their
596 representation in global climate models, Wiley Interdisciplinary Reviews: Climate Change, 8, e465,
597 10.1002/wcc.465, 2017.

598 Chen, Q., Mirrielees, J. A., Thanekar, S., Loeb, N. A., Kirpes, R. M., Upchurch, L. M., Barget, A. J., Lata,
599 N. N., Raso, A. R. W., McNamara, S. M., China, S., Quinn, P. K., Ault, A. P., Kennedy, A., Shepson, P. B.,
600 Fuentes, J. D., and Pratt, K. A.: Atmospheric particle abundance and sea salt aerosol observations in
601 the springtime Arctic: a focus on blowing snow and leads, Atmos. Chem. Phys, 22, 15263-15285,
602 10.5194/acp-22-15263-2022, 2022.

603 Conen, F., Stopelli, E., and Zimmermann, L.: Clues that decaying leaves enrich Arctic air with ice
604 nucleating particles, Atmos. Environ., 129, 91-94, 10.1016/j.atmosenv.2016.01.027, 2016.

605 Creamean, J. M., Kirpes, R. M., Pratt, K. A., Spada, N. J., Maahn, M., de Boer, G., Schnell, R. C., and
606 China, S.: Marine and terrestrial influences on ice nucleating particles during continuous springtime
607 measurements in an Arctic oilfield location, Atmos. Chem. Phys, 18, 18023-18042, 10.5194/acp-18-
608 18023-2018, 2018.

609 Creamean, J. M., Cross, J. N., Pickart, R., McRaven, L., Lin, P., Pacini, A., Hanlon, R., Schmale, D. G.,
610 Ceniceros, J., Aydell, T., Colombi, N., Bolger, E., and DeMott, P. J.: Ice Nucleating Particles Carried
611 From Below a Phytoplankton Bloom to the Arctic Atmosphere, Geophys Res Lett, 46, 8572-8581,
612 10.1029/2019gl083039, 2019.

613 Creamean, J. M., Hill, T. C. J., DeMott, P. J., Uetake, J., Kreidenweis, S., and Douglas, T. A.: Thawing
614 permafrost: an overlooked source of seeds for Arctic cloud formation, Environmental Research
615 Letters, 15, 10.1088/1748-9326/ab87d3, 2020.

616 Creamean, J. M., Barry, K., Hill, T. C. J., Hume, C., DeMott, P. J., Shupe, M. D., Dahlke, S., Willmes, S.,
617 Schmale, J., Beck, I., Hoppe, C. J. M., Fong, A., Chamberlain, E., Bowman, J., Scharien, R., and
618 Persson, O.: Annual cycle observations of aerosols capable of ice formation in central Arctic clouds,
619 Nat Commun, 13, 3537, 10.1038/s41467-022-31182-x, 2022.

620 Daily, M. I., Tarn, M. D., Whale, T. F., and Murray, B. J.: An evaluation of the heat test for the ice-
621 nucleating ability of minerals and biological material, Atmos. Meas. Tech., 15, 2635-2665,
622 10.5194/amt-15-2635-2022, 2022.

623 DeMott, P. J., Hill, T. C., McCluskey, C. S., Prather, K. A., Collins, D. B., Sullivan, R. C., Ruppel, M. J.,
624 Mason, R. H., Irish, V. E., Lee, T., Hwang, C. Y., Rhee, T. S., Snider, J. R., McMeeking, G. R., Dhaniyala,

625   S., Lewis, E. R., Wentzell, J. J., Abbatt, J., Lee, C., Sultana, C. M., Ault, A. P., Axson, J. L., Diaz Martinez,
626   M., Venero, I., Santos-Figueroa, G., Stokes, M. D., Deane, G. B., Mayol-Bracero, O. L., Grassian, V. H.,
627   Bertram, T. H., Bertram, A. K., Moffett, B. F., and Franc, G. D.: Sea spray aerosol as a unique source of
628   ice nucleating particles, Proc Natl Acad Sci U S A, 113, 5797-5803, 10.1073/pnas.1514034112, 2016.
629   Fan, S.-M.: Modeling of observed mineral dust aerosols in the arctic and the impact on winter season
630   low-level clouds, J. Geophys. Res. Atmos., 118, 11,161-111,174, 10.1002/jgrd.50842, 2013.
631   Flyger, H., and Heidam, N. Z.: Ground level measurements of the summer tropospheric aerosol in
632   Northern Greenland, J. Aerosol Sci, 9, 157-168, 10.1016/0021-8502(78)90075-7, 1978.
633   Francis, D., Eayrs, C., Chaboureau, J. P., Mote, T., and Holland, D. M.: Polar Jet Associated Circulation
634   Triggered a Saharan Cyclone and Derived the Poleward Transport of the African Dust Generated by
635   the Cyclone, J. Geophys. Res. Atmos., 123, 11,899-811,917, 10.1029/2018jd029095, 2018.
636   Frey, M. M., Norris, S. J., Brooks, I. M., Anderson, P. S., Nishimura, K., Yang, X., Jones, A. E.,
637   Nerentorp Mastromonaco, M. G., Jones, D. H., and Wolff, E. W.: First direct observation of sea salt
638   aerosol production from blowing snow above sea ice, Atmos. Chem. Phys, 20, 2549-2578,
639   10.5194/acp-20-2549-2020, 2020.
640   Gong, X., Wex, H., van Pinxteren, M., Triesch, N., Fomba, K. W., Lubitz, J., Stolle, C., Robinson, T. B.,
641   Müller, T., Herrmann, H., and Stratmann, F.: Characterization of aerosol particles at Cabo Verde close
642   to sea level and at the cloud level – Part 2: Ice-nucleating particles in air, cloud and seawater, Atmos.
643   Chem. Phys, 20, 1451-1468, 10.5194/acp-20-1451-2020, 2020.
644   Groot Zwaaftink, C. D., Grythe, H., Skov, H., and Stohl, A.: Substantial contribution of northern high-
645   latitude sources to mineral dust in the Arctic, J. Geophys. Res. Atmos., 121, 13,678-613,697,
646   10.1002/2016jd025482, 2016.
647   Gunsch, M. J., Kirpes, R. M., Kolesar, K. R., Barrett, T. E., China, S., Sheesley, R. J., Laskin, A.,
648   Wiedensohler, A., Tuch, T., and Pratt, K. A.: Contributions of transported Prudhoe Bay oil field
649   emissions to the aerosol population in Utqiaġvik, Alaska, Atmos. Chem. Phys, 17, 10879-10892,
650   10.5194/acp-17-10879-2017, 2017.
651   Harrison, A. D., Lever, K., Sanchez-Marroquin, A., Holden, M. A., Whale, T. F., Tarn, M. D., McQuaid,
652   J. B., and Murray, B. J.: The ice-nucleating ability of quartz immersed in water and its atmospheric
653   importance compared to K-feldspar, Atmospheric Chemistry and Physics Discussions, 2019, 1-23,
654   10.5194/acp-2019-288, 2019.
655   Harrison, A. D., O'Sullivan, D., Adams, M. P., Porter, G. C. E., Blades, E., Brathwaite, C., Chewitt-Lucas,
656   R., Gaston, C., Hawker, R., Krüger, O. O., Neve, L., Pöhlker, M. L., Pöhlker, C., Pöschl, U., Sanchez-
657   Marroquin, A., Sealy, A., Sealy, P., Tarn, M. D., Whitehall, S., McQuaid, J. B., Carslaw, K. S., Prospero,
658   J. M., and Murray, B. J.: The ice-nucleating activity of African mineral dust in the Caribbean boundary
659   layer, Atmos. Chem. Phys. Discuss., 2022, 1-34, 10.5194/acp-2022-57, 2022.
660   Hartmann, M., Adachi, K., Eppers, O., Haas, C., Herber, A., Holzinger, R., Hünerbein, A., Jäkel, E.,
661   Jentzsch, C., Pinxteren, M., Wex, H., Willmes, S., and Stratmann, F.: Wintertime Airborne
662   Measurements of Ice Nucleating Particles in the High Arctic: A Hint to a Marine, Biogenic Source for
663   Ice Nucleating Particles, Geophys Res Lett, 47, 10.1029/2020gl087770, 2020.
664   Hartmann, M., Gong, X., Kecorius, S., van Pinxteren, M., Vogl, T., Welti, A., Wex, H., Zeppenfeld, S.,
665   Herrmann, H., Wiedensohler, A., and Stratmann, F.: Terrestrial or marine – indications towards the
666   origin of ice-nucleating particles during melt season in the European Arctic up to 83.7° N, Atmos.
667   Chem. Phys, 21, 11613-11636, 10.5194/acp-21-11613-2021, 2021.
668   Hawker, R. E., Miltenberger, A. K., Wilkinson, J. M., Hill, A. A., Shipway, B. J., Cui, Z., Cotton, R. J.,
669   Carslaw, K. S., Field, P. R., and Murray, B. J.: The temperature dependence of ice-nucleating particle
670   concentrations affects the radiative properties of tropical convective cloud systems, Atmos. Chem.
671   Phys, 21, 5439-5461, 10.5194/acp-21-5439-2021, 2021.
672   Hiranuma, N., Brooks, S. D., Moffet, R. C., Glen, A., Laskin, A., Gilles, M. K., Liu, P., Macdonald, A. M.,
673   Strapp, J. W., and McFarquhar, G. M.: Chemical characterization of individual particles and residuals
674   of cloud droplets and ice crystals collected on board research aircraft in the ISDAC 2008 study, J.
675   Geophys. Res. Atmos., 118, 6564-6579, 10.1002/jgrd.50484, 2013.

676 Hoose, C., and Mohler, O.: Heterogeneous ice nucleation on atmospheric aerosols: a review of
677 results from laboratory experiments, Atmos. Chem. Phys, 12, 9817-9854, 10.5194/acp-12-9817-
678 2012, 2012.
679 Huang, J., and Jaeglé, L.: Wintertime enhancements of sea salt aerosol in polar regions consistent
680 with a sea ice source from blowing snow, Atmos. Chem. Phys, 17, 3699-3712, 10.5194/acp-17-3699-
681 2017, 2017.
682 Huang, Z., Huang, J., Hayasaka, T., Wang, S., Zhou, T., and Jin, H.: Short-cut transport path for Asian
683 dust directly to the Arctic: a case study, Environmental Research Letters, 10, 114018, 10.1088/1748-
684 9326/10/11/114018, 2015.
685 Huneeus, N., Schulz, M., Balkanski, Y., Griesfeller, J., Prospero, J., Kinne, S., Bauer, S., Boucher, O.,
686 Chin, M., Dentener, F., Diehl, T., Easter, R., Fillmore, D., Ghan, S., Ginoux, P., Grini, A., Horowitz, L.,
687 Koch, D., Krol, M. C., Landing, W., Liu, X., Mahowald, N., Miller, R., Morcrette, J. J., Myhre, G.,
688 Penner, J., Perlwitz, J., Stier, P., Takemura, T., and Zender, C. S.: Global dust model intercomparison
689 in AeroCom phase I, Atmos. Chem. Phys, 11, 7781-7816, 10.5194/acp-11-7781-2011, 2011.
690 Irish, V. E., Elizondo, P., Chen, J., Chou, C., Charette, J., Lizotte, M., Ladino, L. A., Wilson, T. W.,
691 Gosselin, M., Murray, B. J., Polishchuk, E., Abbatt, J. P. D., Miller, L. A., and Bertram, A. K.: Ice-
692 nucleating particles in Canadian Arctic sea-surface microlayer and bulk seawater, Atmos. Chem.
693 Phys, 17, 10583-10595, 10.5194/acp-17-10583-2017, 2017.
694 Irish, V. E., Hanna, S. J., Willis, M. D., China, S., Thomas, J. L., Wentzell, J. J. B., Cirisan, A., Si, M.,
695 Leaitch, W. R., Murphy, J. G., Abbatt, J. P. D., Laskin, A., Girard, E., and Bertram, A. K.: Ice nucleating
696 particles in the marine boundary layer in the Canadian Arctic during summer 2014, Atmos. Chem.
697 Phys, 19, 1027-1039, 10.5194/acp-19-1027-2019, 2019.
698 Kanji, Z. A., Ladino, L. A., Wex, H., Boose, Y., Burkert-Kohn, M., Cziczo, D. J., and Krämer, M.:
699 Overview of Ice Nucleating Particles, Meteorological Monographs, 58, 1.1-1.33,
700 10.1175/amsmonographs-d-16-0006.1, 2017.
701 Kirpes, R. M., Bondy, A. L., Bonanno, D., Moffet, R. C., Wang, B., Laskin, A., Ault, A. P., and Pratt, K.
702 A.: Secondary sulfate is internally mixed with sea spray aerosol and organic aerosol in the winter
703 Arctic, Atmos. Chem. Phys, 18, 3937-3949, 10.5194/acp-18-3937-2018, 2018.
704 Kirpes, R. M., Bonanno, D., May, N. W., Fraund, M., Barget, A. J., Moffet, R. C., Ault, A. P., and Pratt,
705 K. A.: Wintertime Arctic Sea Spray Aerosol Composition Controlled by Sea Ice Lead Microbiology, ACS
706 Cent Sci, 5, 1760-1767, 10.1021/acscentsci.9b00541, 2019.
707 Kirpes, R. M., Rodriguez, B., Kim, S., China, S., Laskin, A., Park, K., Jung, J., Ault, A. P., and Pratt, K. A.:
708 Emerging investigator series: influence of marine emissions and atmospheric processing on
709 individual particle composition of summertime Arctic aerosol over the Bering Strait and Chukchi Sea,
710 Environ Sci Process Impacts, 22, 1201-1213, 10.1039/c9em00495e, 2020.
711 Komurcu, M., Storelvmo, T., Tan, I., Lohmann, U., Yun, Y., Penner, J. E., Wang, Y., Liu, X., and
712 Takemura, T.: Intercomparison of the cloud water phase among global climate models, J. Geophys.
713 Res. Atmos., 119, 3372-3400, 10.1002/2013jd021119, 2014.
714 Korolev, A., McFarquhar, G., Field, P. R., Franklin, C., Lawson, P., Wang, Z., Williams, E., Abel, S. J.,
715 Axisa, D., Borrmann, S., Crosier, J., Fugal, J., Krämer, M., Lohmann, U., Schlenczek, O., Schnaiter, M.,
716 and Wendisch, M.: Mixed-Phase Clouds: Progress and Challenges, Meteorological Monographs, 58,
717 5.1-5.50, 10.1175/amsmonographs-d-17-0001.1, 2017.
718 Lewis, E., and Schwartz, S.: Sea Salt Aerosol Production: Mechanisms, Methods, Measurements and
719 Models—A Critical Review, GMS, 152, 3719, 10.1029/GM152, 2004.
720 Lindsley, W. G.: Filter Pore Size and Aerosol Sample Collection, NIOSH Manual of Analytical Methods,
721 1-14, 2016.
722 Mason, R. H., Si, M., Chou, C., Irish, V. E., Dickie, R., Elizondo, P., Wong, R., Brintnell, M., Elsasser, M.,
723 Lassar, W. M., Pierce, K. M., Leaitch, W. R., MacDonald, A. M., Platt, A., Toom-Sauntry, D., Sarda-
724 Esteve, R., Schiller, C. L., Suski, K. J., Hill, T. C. J., Abbatt, J. P. D., Huffman, J. A., DeMott, P. J., and
725 Bertram, A. K.: Size-resolved measurements of ice-nucleating particles at six locations in North
726 America and one in Europe, Atmos. Chem. Phys, 16, 1637-1651, 10.5194/acp-16-1637-2016, 2016.

727   May, N. W., Quinn, P. K., McNamara, S. M., and Pratt, K. A.: Multiyear study of the dependence of
728   sea salt aerosol on wind speed and sea ice conditions in the coastal Arctic, J. Geophys. Res. Atmos.,
729   121, 9208-9219, 10.1002/2016jd025273, 2016.
730   McCluskey, C. S., Ovadnevaite, J., Rinaldi, M., Atkinson, J. D., Belosi, F., Ceburnis, D., Marullo, S., Hill,
731   T. C. J., Lohmann, U., Kanji, Z. A., O'Dowd, C., Kreidenweis, S. M., and DeMott, P. J.: Marine and
732   Terrestrial Organic Ice-Nucleating Particles in Pristine Marine to Continentally Influenced Northeast
733   Atlantic Air Masses, J. Geophys. Res. Atmos., 123, 6196-6212, 10.1029/2017jd028033, 2018.
734   McCoy, D. T., Tan, I., Hartmann, D. L., Zelinka, M. D., and Storelvmo, T.: On the relationships among
735   cloud cover, mixed-phase partitioning, and planetary albedo in GCMs, Journal of Advances in
736   Modeling Earth Systems, 8, 650-668, 10.1002/2015ms000589, 2016.
737   McCoy, D. T., Hartmann, D. L., and Zelinka, M. D.: Chapter 9 - Mixed-Phase Cloud Feedbacks, in:
738   Mixed-Phase Clouds, edited by: Andronache, C., Elsevier, 215-236, 2018.
739   Meinander, O., Dagsson-Waldhauserova, P., Amosov, P., Aseyeva, E., Atkins, C., Baklanov, A., Baldo,
740   C., Barr, S. L., Barzycka, B., Benning, L. G., Cvetkovic, B., Enchilik, P., Frolov, D., Gassó, S., Kandler, K.,
741   Kasimov, N., Kavan, J., King, J., Koroleva, T., Krupskaya, V., Kulmala, M., Kusiak, M., Lappalainen, H.
742   K., Laska, M., Lasne, J., Lewandowski, M., Luks, B., McQuaid, J. B., Moroni, B., Murray, B., Möhler, O.,
743   Nawrot, A., Nickovic, S., O'Neill, N. T., Pejanovic, G., Popovicheva, O., Ranjbar, K., Romanias, M.,
744   Samonova, O., Sanchez-Marroquin, A., Schepanski, K., Semenkov, I., Sharapova, A., Shevnina, E., Shi,
745   Z., Sofiev, M., Thevenet, F., Thorsteinsson, T., Timofeev, M., Umo, N. S., Uppstu, A., Urupina, D.,
746   Varga, G., Werner, T., Arnalds, O., and Vukovic Vimic, A.: Newly identified climatically and
747   environmentally significant high-latitude dust sources, Atmos. Chem. Phys, 22, 11889-11930,
748   10.5194/acp-22-11889-2022, 2022.
749   Ménégoz, M., Voldoire, A., Teyssédre, H., Mélia, D. S. y., Peuch, V. H., and Gouttevin, I.: How does
750   the atmospheric variability drive the aerosol residence time in

751   the Arctic region?, Tellus B: Chemical and Physical Meteorology, 64, 10.3402/tellusb.v64i0.11596,
752   2012.
753   Murray, B. J., O'Sullivan, D., Atkinson, J. D., and Webb, M. E.: Ice nucleation by particles immersed in
754   supercooled cloud droplets, Chem Soc Rev, 41, 6519-6554, 10.1039/c2cs35200a, 2012.
755   Murray, B. J., Carslaw, K. S., and Field, P. R.: Opinion: Cloud-phase climate feedback and the
756   importance of ice-nucleating particles, Atmos. Chem. Phys, 21, 665-679, 10.5194/acp-21-665-2021,
757   2021.
758   O'Sullivan, D., Murray, B. J., Malkin, T. L., Whale, T. F., Umo, N. S., Atkinson, J. D., Price, H. C.,
759   Baustian, K. J., Browse, J., and Webb, M. E.: Ice nucleation by fertile soil dusts: relative importance of
760   mineral and biogenic components, Atmos. Chem. Phys, 14, 1853-1867, 10.5194/acp-14-1853-2014,
761   2014.
762   O'Sullivan, D., Murray, B. J., Ross, J. F., Whale, T. F., Price, H. C., Atkinson, J. D., Umo, N. S., and
763   Webb, M. E.: The relevance of nanoscale biological fragments for ice nucleation in clouds, Sci Rep, 5,
764   8082, 10.1038/srep08082, 2015.
765   Petters, M. D., and Wright, T. P.: Revisiting ice nucleation from precipitation samples, Geophys Res
766   Lett, 42, 8758-8766, 10.1002/2015gl065733, 2015.
767   Porter, G. C. E., Sikora, S. N. F., Adams, M. P., Proske, U., Harrison, A. D., Tarn, M. D., Brooks, I. M.,
768   and Murray, B. J.: Resolving the size of ice-nucleating particles with a balloon deployable aerosol
769   sampler: the SHARK, Atmos. Meas. Tech., 13, 2905-2921, 10.5194/amt-13-2905-2020, 2020.
770   Porter, G. C. E., Adams, M. P., Brooks, I. M., Ickes, L., Karlsson, L., Leck, C., Salter, M. E., Schmale, J.,
771   Siegel, K., Sikora, S. N. F., Tarn, M. D., Vüllers, J., Wernli, H., Zieger, P., Zinke, J., and Murray, B. J.:
772   Highly Active Ice-Nucleating Particles at the Summer North Pole, J. Geophys. Res. Atmos., 127, 28,
773   10.1029/2021jd036059, 2022.
774   Prenni, A. J., Harrington, J. Y., Tjernström, M., DeMott, P. J., Avramov, A., Long, C. N., Kreidenweis, S.
775   M., Olsson, P. Q., and Verlinde, J.: Can Ice-Nucleating Aerosols Affect Arctic Seasonal Climate?,
776   Bulletin of the American Meteorological Society, 88, 541-550, 10.1175/bams-88-4-541, 2007.

777 Prenni, A. J., Demott, P. J., Rogers, D. C., Kreidenweis, S. M., McFarquhar, G. M., Zhang, G., and
778 Poellot, M. R.: Ice nuclei characteristics from M-PACE and their relation to ice formation in clouds,
779 Tellus B, 61, 436-448, 10.1111/j.1600-0889.2009.00415.x, 2009.
780 Price, H. C., Baustian, K. J., McQuaid, J. B., Blyth, A., Bower, K. N., Choularton, T., Cotton, R. J., Cui, Z.,
781 Field, P. R., Gallagher, M., Hawker, R., Merrington, A., Miltenberger, A., Neely Iii, R. R., Parker, S. T.,
782 Rosenberg, P. D., Taylor, J. W., Trembath, J., Vergara-Temprado, J., Whale, T. F., Wilson, T. W.,
783 Young, G., and Murray, B. J.: Atmospheric Ice-Nucleating Particles in the Dusty Tropical Atlantic, J.
784 Geophys. Res. Atmos., 123, 2175-2193, 10.1002/2017jd027560, 2018.
785 Reicher, N., Segev, L., and Rudich, Y.: The Weizmann Supercooled Droplets Observation on
786 a Microarray (WISDOM) and application for ambient dust, Atmos. Meas. Tech., 11, 233-248,
787 10.5194/amt-11-233-2018, 2018.
788 Rinaldi, M., Hiranuma, N., Santachiara, G., Mazzola, M., Mansour, K., Paglione, M., Rodriguez, C. A.,
789 Traversi, R., Becagli, S., Cappelletti, D., and Belosi, F.: Ice-nucleating particle concentration
790 measurements from Ny-Ålesund during the Arctic spring–summer in 2018, Atmos. Chem. Phys, 21,
791 14725-14748, 10.5194/acp-21-14725-2021, 2021.
792 Rogers, D. C., DeMott, P. J., and Kreidenweis, S. M.: Airborne measurements of tropospheric ice-
793 nucleating aerosol particles in the Arctic spring, J. Geophys. Res. Atmos., 106, 15053-15063,
794 10.1029/2000jd900790, 2001.
795 Rolph, G., Stein, A., and Stunder, B.: Real-time Environmental Applications and Display sYstem:
796 READY, Environ. Model. Software, 95, 210-228, 10.1016/j.envsoft.2017.06.025, 2017.
797 Rosenberg, P. D., Dean, A. R., Williams, P. I., Dorsey, J. R., Minikin, A., Pickering, M. A., and Petzold,
798 A.: Particle sizing calibration with refractive index correction for light scattering optical particle
799 counters and impacts upon PCASP and CDP data collected during the Fennec campaign, Atmos.
800 Meas. Tech., 5, 1147-1163, 10.5194/amt-5-1147-2012, 2012.
801 Ryder, C. L., Marenco, F., Brooke, J. K., Estelles, V., Cotton, R., Formenti, P., McQuaid, J. B., Price, H.
802 C., Liu, D. T., Ausset, P., Rosenberg, P. D., Taylor, J. W., Choularton, T., Bower, K., Coe, H., Gallagher,
803 M., Crosier, J., Lloyd, G., Highwood, E. J., and Murray, B. J.: Coarse-mode mineral dust size
804 distributions, composition and optical properties from AER-D aircraft measurements over the
805 tropical eastern Atlantic, Atmos. Chem. Phys, 18, 17225-17257, 10.5194/acp-18-17225-2018, 2018.
806 Sanchez-Marroquin, A., Hedges, D. H. P., Hiscock, M., Parker, S. T., Rosenberg, P. D., Trembath, J.,
807 Walshaw, R., Burke, I. T., McQuaid, J. B., and Murray, B. J.: Characterisation of the filter inlet system
808 on the FAAM BAe-146 research aircraft and its use for size-resolved aerosol composition
809 measurements, Atmos. Meas. Tech., 12, 5741-5763, 10.5194/amt-12-5741-2019, 2019.
810 Sanchez-Marroquin, A., Arnalds, O., Baustian-Dorsi, K. J., Browse, J., Dagsson-Waldhauserova, P.,
811 Harrison, A. D., Maters, E. C., Pringle, K. J., Vergara-Temprado, J., Burke, I. T., McQuaid, J. B., Carslaw,
812 K. S., and Murray, B. J.: Iceland is an episodic source of atmospheric ice-nucleating particles relevant
813 for mixed-phase clouds, Science Advances, 6, eaba8137, 10.1126/sciadv.aba8137, 2020.
814 Sanchez-Marroquin, A., West, L. S., Burke, I. T., McQuaid, J. B., and Murray, B. J.: Mineral and
815 biological ice-nucleating particles above the South East of the British Isles, 2021.
816 Santl-Temkiv, T., Lange, R., Beddows, D., Rauter, U., Pilgaard, S., Dall'Osto, M., Gunde-Cimerman, N.,
817 Massling, A., and Wex, H.: Biogenic Sources of Ice Nucleating Particles at the High Arctic Site Villum
818 Research Station, Environ Sci Technol, 53, 10580-10590, 10.1021/acs.est.9b00991, 2019.
819 Schnell, R. C.: Airborne ice nucleus measurements around the Hawaiian Islands, J. Geophys. Res., 87,
820 8886, 10.1029/JC087iC11p08886, 1982.
821 Shi, Y., Liu, X., Wu, M., Ke, Z., and Brown, H.: Relative Importance of High-Latitude Local and Long-
822 Range Transported Dust to Arctic Ice Nucleating Particles and Impacts on Arctic Mixed-Phase Clouds,
823 Atmos. Chem. Phys. Discuss., 2021, 1-57, 10.5194/acp-2021-621, 2021.
824 Shi, Y., Liu, X., Wu, M., Zhao, X., Ke, Z., and Brown, H.: Relative importance of high-latitude local and
825 long-range-transported dust for Arctic ice-nucleating particles and impacts on Arctic mixed-phase
826 clouds, Atmos. Chem. Phys, 22, 2909-2935, 10.5194/acp-22-2909-2022, 2022.

Si, M., Evoy, E., Yun, J., Xi, Y., Hanna, S. J., Chivulescu, A., Rawlings, K., Veber, D., Platt, A., Kunkel, D., Hoor, P., Sharma, S., Leaitch, W. R., and Bertram, A. K.: Concentrations, composition, and sources of ice-nucleating particles in the Canadian High Arctic during spring 2016, Atmos. Chem. Phys, 19, 3007-3024, 10.5194/acp-19-3007-2019, 2019.

Soo, J. C., Monaghan, K., Lee, T., Kashon, M., and Harper, M.: Air sampling filtration media: Collection efficiency for respirable size-selective sampling, Aerosol Sci Technol, 50, 76-87, 10.1080/02786826.2015.1128525, 2016.

Stein, A. F., Draxler, R. R., Rolph, G. D., Stunder, B. J. B., Cohen, M. D., and Ngan, F.: NOAA's HYSPLIT Atmospheric Transport and Dispersion Modeling System, Bulletin of the American Meteorological Society, 96, 2059-2077, 10.1175/bams-d-14-00110.1, 2015.

Storelvmo, T., Tan, I., and Korolev, A. V.: Cloud Phase Changes Induced by CO2 Warming—a Powerful yet Poorly Constrained Cloud-Climate Feedback, Current Climate Change Reports, 1, 288-296, 10.1007/s40641-015-0026-2, 2015.

Tan, I., Storelvmo, T., and Zelinka, M. D.: Observational constraints on mixed-phase clouds imply higher climate sensitivity, Science, 352, 224-227, 10.1126/science.aad5300, 2016.

Tobo, Y., Adachi, K., DeMott, P. J., Hill, T. C. J., Hamilton, D. S., Mahowald, N. M., Nagatsuka, N., Ohata, S., Uetake, J., Kondo, Y., and Koike, M.: Glacially sourced dust as a potentially significant source of ice nucleating particles, Nat Geosci, 12, 253-+, 10.1038/s41561-019-0314-x, 2019.

Ullrich, R., Hoose, C., Mohler, O., Niemand, M., Wagner, R., Hohler, K., Hiranuma, N., Saathoff, H., and Leisner, T.: A New Ice Nucleation Active Site Parameterization for Desert Dust and Soot, J. Atmospheric Sci., 74, 699-717, 10.1175/Jas-D-16-0074.1, 2017.

Vali, G.: Quantitative Evaluation of Experimental Results an the Heterogeneous Freezing Nucleation of Supercooled Liquids, J. Atmospheric Sci., 28, 402-409, 10.1175/1520-0469(1971)028<0402:QEOERA>2.0.CO;2, 1971.

Vali, G.: Revisiting the differential freezing nucleus spectra derived from drop-freezing experiments: methods of calculation, applications, and confidence limits, Atmos. Meas. Tech., 12, 1219-1231, 10.5194/amt-12-1219-2019, 2019.

VanCuren, R. A., Cahill, T., Burkhart, J., Barnes, D., Zhao, Y., Perry, K., Cliff, S., and McConnell, J.: Aerosols and their sources at Summit Greenland – First results of continuous size- and time-resolved sampling, Atmos. Environ., 52, 82-97, 10.1016/j.atmosenv.2011.10.047, 2012.

Vergara-Temprado, J., Murray, B. J., Wilson, T. W., O'Sullivan, D., Browse, J., Pringle, K. J., Ardon-Dryer, K., Bertram, A. K., Burrows, S. M., Ceburnis, D., DeMott, P. J., Mason, R. H., O'Dowd, C. D., Rinaldi, M., and Carslaw, K. S.: Contribution of feldspar and marine organic aerosols to global ice nucleating particle concentrations, Atmos. Chem. Phys, 17, 3637-3658, 10.5194/acp-17-3637-2017, 2017.

Vergara-Temprado, J., Miltenberger, A. K., Furtado, K., Grosvenor, D. P., Shipway, B. J., Hill, A. A., Wilkinson, J. M., Field, P. R., Murray, B. J., and Carslaw, K. S.: Strong control of Southern Ocean cloud reflectivity by ice-nucleating particles, Proc Natl Acad Sci U S A, 115, 2687-2692, 10.1073/pnas.1721627115, 2018.

Welti, A., Bigg, E. K., DeMott, P. J., Gong, X., Hartmann, M., Harvey, M., Henning, S., Herenz, P., Hill, T. C. J., Hornblow, B., Leck, C., Löffler, M., McCluskey, C. S., Rauker, A. M., Schmale, J., Tatzelt, C., van Pinxteren, M., and Stratmann, F.: Ship-based measurements of ice nuclei concentrations over the Arctic, Atlantic, Pacific and Southern oceans, Atmos. Chem. Phys, 20, 15191-15206, 10.5194/acp-20-15191-2020, 2020.

Wex, H., Huang, L., Zhang, W., Hung, H., Traversi, R., Becagli, S., Sheesley, R. J., Moffett, C. E., Barrett, T. E., Bossi, R., Skov, H., Hünerbein, A., Lubitz, J., Löffler, M., Linke, O., Hartmann, M., Herenz, P., and Stratmann, F.: Annual variability of ice-nucleating particle concentrations at different Arctic locations, Atmos. Chem. Phys, 19, 5293-5311, 10.5194/acp-19-5293-2019, 2019.

Whale, T. F., Murray, B. J., O'Sullivan, D., Wilson, T. W., Umo, N. S., Baustian, K. J., Atkinson, J. D., Workneh, D. A., and Morris, G. J.: A technique for quantifying heterogeneous ice nucleation in

877 microlitre supercooled water droplets, Atmos. Meas. Tech., 8, 2437-2447, 10.5194/amt-8-2437-
878 2015, 2015.
879 Wilson, T. W., Ladino, L. A., Alpert, P. A., Breckels, M. N., Brooks, I. M., Browse, J., Burrows, S. M.,
880 Carslaw, K. S., Huffman, J. A., Judd, C., Kilthau, W. P., Mason, R. H., McFiggans, G., Miller, L. A.,
881 Najera, J. J., Polishchuk, E., Rae, S., Schiller, C. L., Si, M., Vergara-Temprado, J., Whale, T. F., Wong, J.
882 P., Wurl, O., Yakobi-Hancock, J. D., Abbatt, J. P., Aller, J. Y., Bertram, A. K., Knopf, D. A., and Murray,
883 B. J.: A marine biogenic source of atmospheric ice-nucleating particles, Nature, 525, 234-238,
884 10.1038/nature14986, 2015.
885 Yang, X., Pyle, J. A., and Cox, R. A.: Sea salt aerosol production and bromine release: Role of snow on
886 sea ice, Geophys Res Lett, 35, 1-5, 10.1029/2008gl034536, 2008.
887 Young, G., Jones, H. M., Darbyshire, E., Baustian, K. J., McQuaid, J. B., Bower, K. N., Connolly, P. J.,
888 Gallagher, M. W., and Choularton, T. W.: Size-segregated compositional analysis of aerosol particles
889 collected in the European Arctic during the ACCACIA campaign, Atmos. Chem. Phys, 16, 4063-4079,
890 DOI 10.5194/acp-16-4063-2016, 2016.
891 Yun, J., Evoy, E., Worthy, S. E., Fraser, M., Veber, D., Platt, A., Rawlings, K., Sharma, S., Leaitch, W. R.,
892 and Bertram, A.: Ice nucleating particles in the Canadian High Arctic during the fall of 2018,
893 Environmental Science: Atmospheres, 10.1039/d1ea00068c, 2022.
894 Zhao, X., Huang, K., Fu, J. S., and Abdullaev, S. F.: Long-range transport of Asian dust to the Arctic:
895 identification of transport pathways, evolution of aerosol optical properties, and impact assessment
896 on surface albedo changes, Atmos. Chem. Phys, 22, 10389-10407, 10.5194/acp-22-10389-2022,
897 2022.
898
899